NMR-Controlled Titrations: Characterizing Aminophosphonates and Related Structures

Gerhard Hägele, Zoltán Szakács, Johannes Ollig, Stephan Hermens, and Christian Pfaff

Institut für Anorganische Chemie, Heinrich-Heine-Universität Düsseldorf Universitätsstraße 1, D-40225-Düsseldorf, Germany; haegele@uni-duesseldorf.de

Received 15 September 2000

ABSTRACT: *Aminophosphonic acids, aminophosphinic acids, and aminophosphonous acids give rise to interesting protonation and metal complex formation equilibria, which can be monitored by potentiometric and NMR spectroscopic methods. A hyphenated technique referred to as NMR-controlled titrations or titration-dependent NMR spectroscopy has been introduced. Vicinal and geminal bisphosphonic acids have also been characterized by this method. Gradients (titration shifts) in chemical shifts and coupling constants were used to elucidate the structures of the protolytic species. Microscopic dissociation equilibria have also been studied by NMR-controlled titrations for glufosinate and 4-aminophenylphosphonic acid. Some comments are made on the UV-vis-controlled titration of the latter compound. Novel, advanced algorithms were used to estimate the error of analytical and NMR parameters, such as pK values, molar fractions, and ion-specific chemical shifts, describing the aminophosphonate ligands in each protonation form.* © 2000 John Wiley & Sons, Inc. Heteroatom Chem 11:562–582, 2000

INTRODUCTION

Analytical and NMR spectroscopic aspects of aminophosphonates and related structures have attracted considerable attention [1]. Protolytic and

metal complex formation of compounds of biological and technical relevance were studied by potentiometric methods. NMR methods were used to elucidate structures of neutral and ionic species formed, or synthetic routes, yields, and more simply, purity of practical products.

The aim of this article is to demonstrate an automated, hyphenated technique combining both aspects: potentiometric titration and NMR spectroscopy. This hyphenation leads conveniently to two- and three-dimensional graphical representations where NMR parameters are correlated with analytical parameters. This method may be termed as NMR-controlled titration or titration-dependent NMR spectroscopy. NMR-controlled titrations yield characteristic dissociation and stability constants, NMR parameters such as resonance frequencies, chemical shifts, and coupling constants for the individual species involved in macroscopic or, in fortunate cases also, microscopic equilibria. NMR-controlled titration is an efficient tool to characterize aminophosphonates and related structures using resonances from standard $^{31}P\{^1H\}$, $^{13}C\{^1H\}$, $^1H\{^{31}P\}$, and ^1H NMR. ^{19}F NMR is applied to study fluorinated aminophosphonates and in favorable cases metal-NMR spectroscopy may monitor metal complex formation.

THEORY

Macroscopic Protolytic Equilibria-Dissociation- and Stability Constants

Consider an amino acid where the number of acidic functions (e.g., C(O)OH, P(O)OH, etc.) is repre-

sented by a, anionic, and b, the number of basic functions (e.g., NH_2, NHR, NR_2, etc.). This situation corresponds with the general description of a n-valent base L^{-a} having (a) anionic and (b) neutral base centers $(^0N)_b\text{-R-}(O^-)_a$. Full protonation leads to (a) n-valent acid H_nL^{n-a} ($n = a + b$) having a neutral and (b) cationic acid centers $(^+HN)_b\text{-R-}(OH^0)_a$. Table 1 exemplifies this concept on all the compounds that we discuss in this study.

Salts may be defined in a general way as $H_{a-x+y}X_xLY_y$, where X and Y stand for univalent ions bearing either positive or negative charges, as shown in Table 2.

The protonation equilibrium of an n-valent base is described by the reactions:

$$iH^+ + L^{-a} = H_iL^{i-a} \quad (i = 1, 2, ..., n) \quad (1)$$
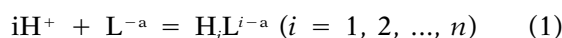
and by brutto stability constants:

$$\beta_i = \frac{c_{H_iL^{i-a}}}{c_{H^+}^i \cdot c_{L^{a-}}} \quad (i = 0 - n) \quad (2)$$

The β_i data are connected with the stepwise acid and base dissociation constants K_{a_i} and K_{b_i} by the logarithmic expressions:

(a) $pK_{a_i} = -\log \beta_{n+1-i} + \log \beta_{n-i};$

(b) $\log \beta_i = \sum_{j=1}^{i} pK_{a_{n+1-j}};$

(c) $pK_{b_i} = i \cdot pK_W - \log \beta_i + \log \beta_{i-1};$

(d) $\log \beta_i = i \cdot pK_W - \sum_{j=1}^{i} pK_{b_j}. \quad (3)$

In this article, stoichiometric variables (containing concentrations instead of activities) are used in abbreviated forms: pK_i (macroscopic acid dissociation constant), pk_i (microscopic acid dissociation constant), pK_W (ion product of water). pH stands always for the concentration-based pcH = $^{10}\log(c_H)$. Glass electrodes are calibrated by blank titration in terms of pcH (see following section).

The molar fractions of the protolytic species are derived:

$$\chi_i = \frac{10^{(lg\beta_i - i \cdot pH)}}{\sum_{k=0}^{n} 10^{(lg\beta_k - k \cdot pH)}} \quad (4)$$

Each species H_iL^{i-a} present in the equilibrium contributes ion-specific NMR parameters $\delta_{H_iL^{i-a}}$ in an exchange reaction that is rapid on the NMR timescale. Effectively, only one signal is observed when monitoring $^{31}P\{^1H\}$-NMR during the course of titrations. An averaged chemical shift $\langle\delta\rangle$ appears following:

$$\langle\delta\rangle = \sum_{i=0}^{n} x_i\delta_{H_iL^{i-a}} \quad (5)$$

It is useful to introduce a quantity called the titration shift $\Delta\delta$, following:

$$\Delta\delta_j = \delta_j - \delta_{j+1} \quad (6)$$

where j indicates a particular state of titration, e.g. protonation, deprotonation, metal complex formation, etc. For our purposes, in this report it suffices to introduce the definition of deprotonation gradients Δ_i (ppm) given by:

$$\Delta_i = \delta_{H_iL} - \delta_{H_{i-1}L} \quad (7)$$

Here a gradient defines the change of chemical shift per proton abstracted. We will show that their signs and magnitudes are indicative in many favorable cases to elucidate the deprotonation and protonation pathways of multidentate ligands.

The dynamically averaged chemical shift $\langle\delta\rangle$ is a function of pcH. Experimentally, the pcH of solutions may be varied by two methods: (a) titration with a strong univalent acid (HCl) or (b) with a strong univalent base (NaOH). While the experiment directly provides the well-known titration curve pcH $= f(V_2)$, it is more convenient to calculate its inverse $V_2 = f(pcH)$ by computer programs.

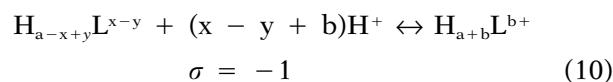The variables for volumes (mL) and concentrations (mol/L) are listed in Table 3.

Using these quantities and the following expressions,

$$A = 10^{-pH} - 10^{pK_W - pH} \quad (8)$$

$$B = (x - y) + \sum_{i=0}^{n} (i - a) \cdot \chi_i \quad (9)$$

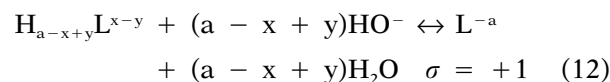we can describe titrations:

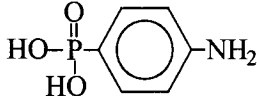(a) with a strong acid, for example, HCl, HNO_3, or $HClO_4$:

$$H_{a-x+y}L^{x-y} + (x - y + b)H^+ \leftrightarrow H_{a+b}L^{b+}$$
$$\sigma = -1 \quad (10)$$

$$V_{A2} = A(V_{L1} + V_{A1} + V_{B1} + V_{I1} + V_{W1})$$
$$+ V_{B1}C_{B1} - V_{A1}C_{A1}$$
$$+ V_{L1}C_{L1}B/C_{A2} - A \quad (11)$$

(b) with a strong base, for example, NaOH or tetramethylammonium hydroxide (TMAOH):

$$H_{a-x+y}L^{x-y} + (a - x + y)HO^- \leftrightarrow L^{-a}$$
$$+ (a - x + y)H_2O \quad \sigma = +1 \quad (12)$$

$$V_{B2} = A(V_{L1} + V_{A1} + V_{B1} + V_{I1} + V_{W1})$$
$$+ V_{B1}C_{B1} - V_{A1}C_{A1}$$
$$+ V_{L1}C_{L1}B/C_{B2} + A \quad (13)$$

TABLE 1 Classification of the Aminophosphonates and Related Structures Studied

Compound	Formula	Abbreviation	a	b	n
1	$CH_3-\underset{\underset{NH_2}{\mid}}{CH}-PO_3H_2$	α-Ala-P	2	1	3
2	$\underset{\underset{NH_2}{\mid}}{CH_2}-CH_2-PO_3H_2$	β-Ala-P	2	1	3
3	$H_2O_3P-CH_2-\underset{\underset{NH_2}{\mid}}{CH}-PO_3H_2$	Asp-P$_2$	4	1	5
4	$CF_3-\underset{\underset{NH_2}{\mid}}{CH}-PO_3H_2$	F-α-Ala-P	2	1	3
5	$\underset{\underset{NH_2}{\mid}}{CH_2}-CH_2-\underset{\underset{CH_3}{\mid}}{P}(O)(OH)$	β-Ala-P$'$	1	1	2
6	$CH_3-CH_2-\underset{\underset{NH_2}{\mid}}{CH}-PH(O)(OH)$	APP$''$	1	1	2
7	$CH_3-\underset{\underset{PO_3H_2}{\mid}}{\overset{\overset{PO_3H_2}{\mid}}{C}}-OH$	HEDP	4	0	4
8	$\underset{\underset{NH_2}{\mid}}{CH_2}-CH_2-\underset{\underset{PO_3H_2}{\mid}}{\overset{\overset{PO_3H_2}{\mid}}{C}}-OH$	Pamidronate	4	1	5
9	$\underset{\underset{NH_2}{\mid}}{CH_2}-CH_2-CH_2-\underset{\underset{PO_3H_2}{\mid}}{\overset{\overset{PO_3H_2}{\mid}}{C}}-OH$	Alendronate	4	1	5
10	$CH_3-CH_2-NH-CH_2-\underset{\underset{CH_3}{\mid}}{P}(O)OH$	EAMP$'$	1	1	2
11	$HO-\underset{\underset{HO}{\mid}}{\overset{\overset{O}{\parallel}}{P}}-\bigcirc-NH_2$	APHP	2	1	3
12	$\underset{\underset{NH_2}{\mid}}{CH_2}-CH_2-CH_2-PO_3H_2$	APP	2	1	3
13	$HO(O)\underset{\underset{H_3C}{\mid}}{P}-CH_2-CH_2-\underset{\underset{NH_2}{\mid}}{CH}-COOH$	Glufosinate	2	1	3

For systematic names, see Experimental section.

TABLE 2 Classification of Salts Derived from Aminophosphonates

Case	Type	X	x	Y	y
1	Sodium salt	Na^+	$1 < x \leq a$	—	0
2	Hydrogenchloride salt	—	0	Cl^-	$1 < y < b$

TABLE 3 Analytical Parameters Used to Describe Acid-Base Titration

	Volume	Concentration	Type
Titrand	V_{L1}	C_{L1}	Acid/Base/Salt of Ligand L
	V_{A1}	C_{A1}	Univalent strong acid, e.g. HCl
	V_{B1}	C_{B1}	Univalent strong base, e.g. NaOH
	V_{11}	C_{11}	Ion buffer 1:1, e.g. NaCl
	V_{W1}		Water for dilution
Titrator	V_{B2}	C_{B2}	Univalent strong base, e.g. NaOH
	V_{A2}	C_{A2}	Univalent strong acid, e.g. HCl

A more convenient and general expression for the volume of titrator, V_2, is obtained using the σ parameter:

$$V_2 = A(V_{L1} + V_{A1} + V_{B1} + V_{I1} + V_{W1})$$
$$+ V_{B1}C_{B1} - V_{A1}C_{A1}$$
$$+ V_{L1}C_{L1}B/C_2 + \sigma A \quad (14)$$

It is useful to define a parameter for the degree of titration, τ:

$$\tau = \frac{(V_{B1}C_{B1} - V_{A1}C_{A1}) + V_2(C_{B2} - C_{A2})}{V_{L1}C_{L1}}$$
$$+ x - y \quad (15)$$

Complex Formation Equilibria: Macroscopic Conditional Stability Constants

Complex formation involving the three components L^{n-}, H^+, and M^{m+} leading to nsp species of the ith type $M_{p_i}H_{q_i}L_{r_i}$ may be described briefly (neglecting the ionic charges) by

$$p_iM + q_iH + r_iL = M_{p_i}H_{q_i}L_{r_i} \quad (16)$$
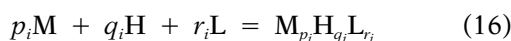
$$\beta_{p_iq_ir_i} = \frac{c_{M_{p_i}H_{q_i}L_{r_i}}}{c_M^{p_i} \cdot c_H^{q_i} \cdot c_L^{r_i}} \quad (17)$$

and the fundamental equations:

$$C_M^t = c_M + \sum_{i=1}^{nsp} p_i \cdot \beta_{p_iq_ir_i} \cdot c_M^{p_i} \cdot c_H^{q_i} \cdot c_L^{r_i} \quad (18)$$

$$C_L^t = c_L + \sum_{i=1}^{nsp} r_i \cdot \beta_{p_iq_ir_i} \cdot c_M^{p_i} \cdot c_H^{q_i} \cdot c_L^{r_i} \quad (19)$$

$$C_S^t - C_B^t = c_H - \frac{K_W}{c_H} + \sum_{i=1}^{nsp} q_i \cdot \beta_{p_iq_ir_i}$$
$$\cdot c_M^{p_i} \cdot c_H^{q_i} \cdot c_L^{r_i} \quad (20)$$

Equations 18–20 are solved numerically in free-component concentrations c_M, c_H, and c_L for given $\beta_{p_iq_ir_i}$ and actual total concentrations C_M^t and C_L^t; $C_S^t - C_B^t$ stand for the univalent acid and base used in titrand and titrator, respectively.

Several methods and programs have been developed in the literature to simulate titration curves for complex formation equilibria [2–4]. Restricting $p = 1$, $q = 1$ or 2, with arbitrary r, simple algebraic equations are derived for fast simulations with GENCOM [5a]. Cumulative stability constants $\beta_{p_iq_ir_i}$ are obtained by iterative least-square treatment of titration data [2–4]. A convenient menu-driven PC-iterator ITERAX [5b] was designed in TURBO PASCAL based upon BEST [3], which accepts the data output from automated titrations. If $p = 0$ and $r = 1$, then the protonation of the free ligands will be covered by Equations 1, 2, and 4 and ($c_M = 0$) and the corresponding programs. This simplified situation allows for an explicit algebraic solution of the titration problem.

Each component and the species $M_{p_i}H_{q_i}L_{r_i}$ present in the equilibrium contributes ion-specific NMR parameters, $\delta_{M_{p_i}H_{q_i}L_{r_i}}$, in an exchange reaction that is rapid on the NMR timescale. One signal only is observed, for example, when monitoring $^{31}P\{^1H\}$-NMR during the course of our titrations using phosphonate compounds. On the other hand, discrete NMR signals may be observed for kinetically inert complexes.

If we monitor the ligand L by NMR, an averaged chemical shift $\langle \delta_L \rangle$ appears following:

$$\langle \delta_L \rangle = \sum_{i=0}^{n} x_i r_i \delta_{M_{p_i}H_{q_i}L_{r_i}} \quad (21)$$

Analogously monitoring the metal M, an averaged chemical shift $\langle \delta_M \rangle$ will follow:

$$\langle \delta_M \rangle = \sum_{i=0}^{n} x_i p_i \delta_{M_{p_i}H_{q_i}L_{r_i}} \quad (22)$$

NMR-Controlled Titrations Lead to Graphical Representations of Two-Dimensional NMR Type

NMR-controlled titrations are represented by two typical correlations: the τ,δ and the pH,δ plots. For so-called first-order acids, where $pK_{i+1} - pK_i > 3$, a

simple situation holds: the first derivative of $\langle\delta\rangle$ with pcH $d\langle\delta\rangle/dpH$ shows extrema while the second derivative $d^2\langle\delta\rangle/dpH^2$ is zero for pH $=$ pK_i. Consequently pK_i and $\log\beta_i$ are readily obtained in such situations. Second-order cases with $pK_{i+1} - pK_i < 3$ require a full iterative treatment of titration data by suitable methods and programs that are beyond the scope of this article [3,4].

EXPERIMENTAL

Chemicals

The structural formulas of the investigated compounds are listed in Table 1. Some of them were prepared in our group: 2,2,2-trifluoro-1-amino-ethanephosphonic acid **4** (F-α-Ala-P) [6a], (2-aminoethyl)-methylphosphinic acid **5** (β-Ala-P$'$) [6b] and (N-ethyl-aminomethyl)-methylphosphinic acid **10** (EAMP$'$) [6c]. 1-aminoethanephosphonic acid **1** (α-Ala-P) and 2-aminoethanephosphonic acid **2** (β-Ala-P, Ciliatin) were obtained from the Wroclaw team (P. Mastalerz and R. Tyka), while 1-aminoethane-1,2-bisphosphonic acid **3** (diphosphaasparaginic acid, Asp-P$_2$) and 1-aminopropanephosphonous acid **6** (APP$''$) were provided by H. Hudson. 2-Amino-4-(methylphosphino)-butanoic acid **13** (glufosinate, phosphinothricine) was a gift of Hoechst, while 1-hydroxyethane-1,1-diphosphonic acid **7** (HEDP), 3-amino-1-hydroxypropane-1,1-diphosphonic acid **8** (pamidronic acid) and 4-amino-1-hydroxybutane-1,1-diphosphonic acid **9** (alendronic acid) were supplied by Henkel. 4-Aminophenylphosphonic acid **11** (phosphanylic acid, APHP) was purchased from Aldrich, and 3-aminopropanephosphonic acid **12** (APP) from EGA Chemie.

Methods

pK values and $\log\beta$ complex stability constants have been determined by potentiometric titrations under standard experimental conditions: $25.0 \pm 0.1°C$ temperature and 0.1 M ionic strength (adjusted with addition of $NaNO_3$, NaCl, or tetramethylammonium chloride [TMACl]). The ligand concentration varied typically between 0.002 and 0.008 M. A detailed description of our titration apparatus and method can be found in the literature [5c,7a].

The experimental setups for NMR-controlled titrations were developed starting as of early 1988 by the Düsseldorf team [5d,7]. The typical hardware is depicted in Figure 1.

A PC-guided automated cycle is applied to add the titrator, stir, check constancy of temperature and pcH, and to monitor and store the free induction
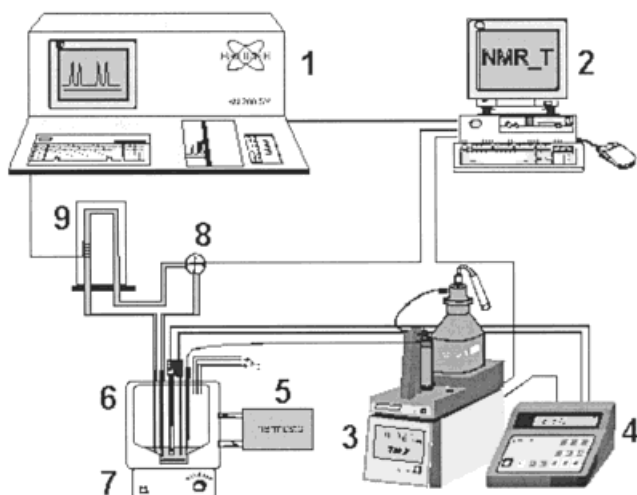
FIGURE 1 Hardware setup for NMR-controlled titrations: (1) NMR-spectrometer; (2) master PC; (3) motor burette; (4) Sensor electrode and potentiometer; (5) thermostat; (6) titration vessel (thermo-controlled, protective gas: N_2 or Ar); (7) magnetic stirrer; (8) PC-guided pump; (9) flow-NMR-probe head, model 1996, BRUKER-NMR-spectrometer SY200.

decays. After sequential Fourier transformation, resulting spectra are phase corrected and stored together with titration data (V_2, τ, pH), as a set of absorption spectra in pseudo-2D-NMR-format and finally processed as stacked or contour plots. The software package serving the 1996 hardware is called NMR_T [5a]. A new, modified version of NMR T shown in Figure 2 below was developed in 1999/2000 in order to serve the BRUKER AVANCE 500 spectrometer [8].

The experimental conditions in NMR-controlled titrations were similar to those in potentiometry, except the temperature ($22 \pm 1°C$) and the ligand concentration (0.01 M in $^{31}P\{^1H\}$ and at least 0.1 M in ^{13}C). For a typical experiment, see HEDP.

RESULTS

$^{31}P\{^1H\}$-NMR Studies on Simple Aminophosphonates

*1-Aminoethanephosphonic acid (**1**) and 2-aminoethanephosphonic acid (**2**).* Protolytic Equilibria. The contour plot for the $^{31}P\{^1H\}$-NMR-controlled titration of **1** is shown in Figure 3 [7a]. Since pK_1 is as low as 0.31, virtually no change in δ_P is observed for $-0.8 < \tau < 0$. The cation H_3L^+ is scarcely populated within this range, henceforth the titrator base added is consumed basically for the reaction $H^+ + OH^- \rightarrow H_2O$ and not for the deprotonation of a POH
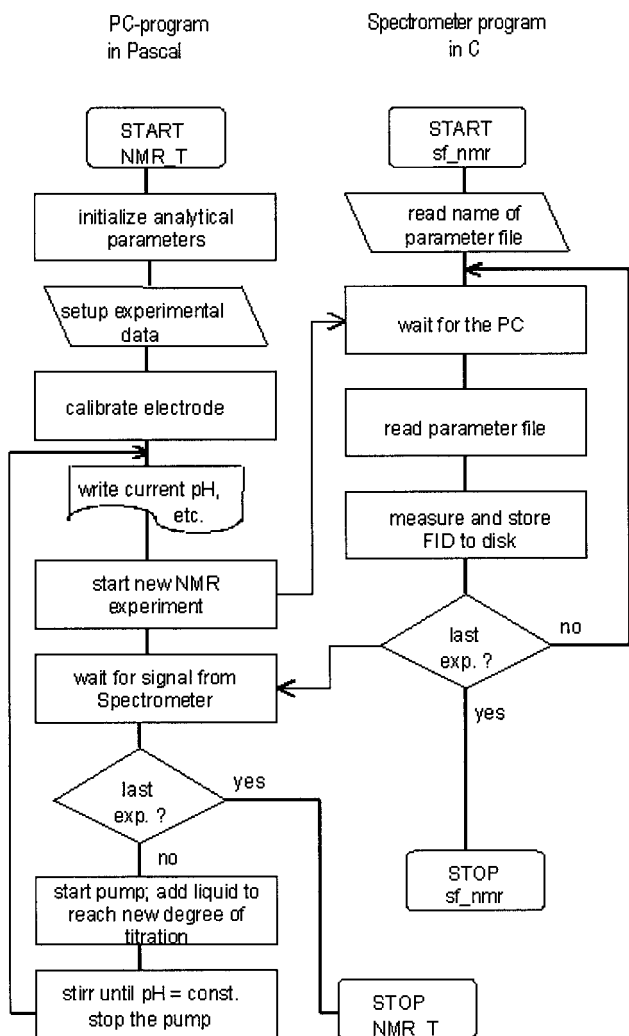
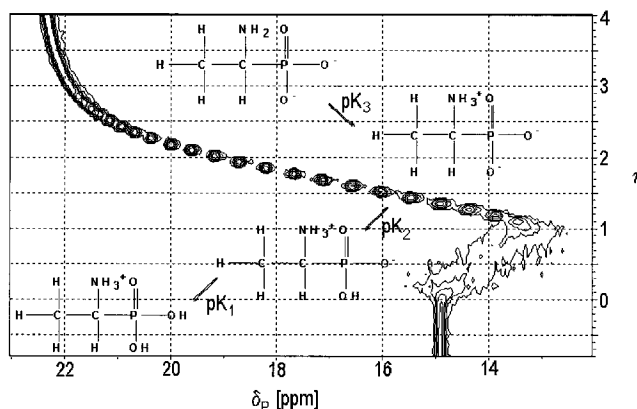FIGURE 2   Software set up for NMR-controlled titrations: program system NMR__T, model 1999 for BRUKER-NMR-spectrometer AVANCE 500.
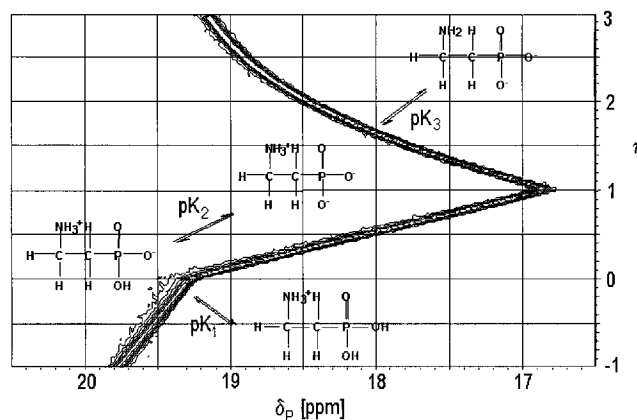

FIGURE 3   81 MHz ^{31}P{^{1}H}-NMR-controlled titration of α-Ala-P **1** with NaOH. Prior to titration, 0.8 equivalents of HNO$_3$ were added to the titrand.

TABLE 4   Ion-Specific ^{31}P Chemical Shifts δ_{H_iL} (ppm) and Protonation Gradients Δ_i (ppm) for α-Ala-P **1** and β-Ala-P **2** Using NaOH and Tetramethylammonium Hydroxide (TMAOH) as Titrator

Ion-Specific Chemical Shift	**1** with NaOH	**2** with NaOH	**2** with TMAOH
$\delta_{H_3L^+}{}^a$	^{b}	23.4	22.9
δ_{H_2L}	14.92	19.26	19.29
δ_{HL^-}	13.08	16.81	16.80
$\delta_{L^{2-}}$	22.25	19.72	19.39
Δ_3	^{b}	4.14	3.61
Δ_2	1.84	2.45	2.49
Δ_1	-9.17	-2.91	-2.59

$^a\delta_{H_3L^+}$ ca. 16 ppm.
^{b}Not iterated values

group. Between $0 < \tau < 1$, a deprotonation shift from $\delta_P = 14.8$ ppm to $\delta_P = 13.2$ ppm occurs, which is significant for the deprotonation of the second POH-group (p$K_2 = 5.63$). Finally, above $\tau > 1$, deprotonation takes place on the NH$_3^+$-group (p$K_3 = 10.21$).

The program AMPLSQ9 [5d,7a] was used to evaluate numerical data for ion-specific chemical shifts. These results, together with data for the analogue compound **2**, which will be discussed below, are listed in Table 4.

A characteristic pattern is observed for ^{31}P{^{1}H}-NMR-controlled titration of the β-analogue **2** [7a], shown in Figure 4.

Here we detect a change of chemical shift δ_P in the region spanning $\tau = -1.0$ and $\tau = 0.0$, because p$K_1 = 1.14$ is significantly higher than the pK_1 of **1**. Analogous remarks hold for p$K_2 = 6.34$ and p$K_3 =$
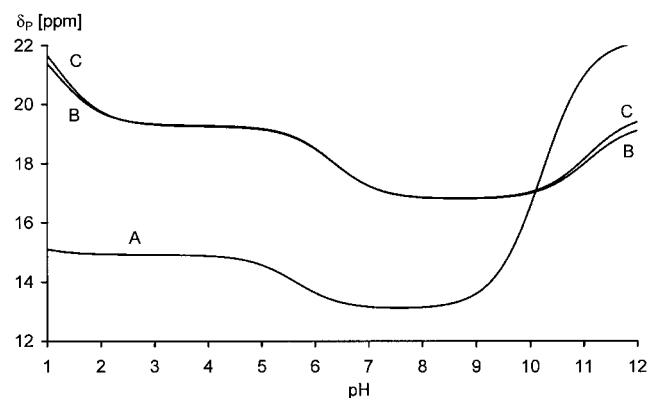

FIGURE 4   81 MHz ^{31}P{^{1}H}-NMR-controlled titration of β-Ala-P **2** with TMAOH. Prior to titration, 1-equivalent of HNO$_3$ was added to the titrand.

11.06. A characteristic decrease of δ_P between $\tau = 0.0$ and $\tau = 1.0$ from $\delta = 19.25$ ppm to $\delta = 16.85$ ppm indicates deprotonation on the POH-group. For $\tau > 1$ the signal shifts to low-field as a result of the deprotonation of the NH_3^+-group. The phosphorus resonance line widths are much broader for **1** than for **2** within the region $0 < \tau < 1$, as can be seen in Figures 3 and 4. This possibly indicates different proton-bridges in betainic structures.

Averaged chemical shifts $\langle\delta\rangle$, ion-specific chemical shifts δ_{H_iL}, dissociation and stability constants given as pK, and log β data obtained from NMR-controlled titrations depend on the nature of cations chosen for bases or ion buffers (see Table 4 and Figure 5). Weak interactions can be expected to occur between the complexing ligands and alkali metal cations. In principle, the protolytic equilibria are overlaid by complex formation processes. Such complications are, however, circumvented using TMAOH as a base and tetramethylammonium salts as ionic buffers.

The pH-δ correlation diagrams for the dynamically averaged chemical shifts of both ligands were simulated with APBPLT [5e] using the data given above and shown in Figure 5. The inflection points mark clearly the individual pK_i values when projected onto the pH axis in Figure 5.

Complex Formation. α-Ala-P **1** and Zn^{2+} form the complexes ML (logβ = 5.45), MHL (logβ = 12.10) and ML_2 (logβ = 12.42), as deduced from potentiometric studies by us [7a] and others [9,10]. The $^{31}P\{^1H\}$-NMR-controlled titration diagram in the presence of zinc (Figure 6) differs from the ligand-only case (Figure 3), indicating a dynamic averaging, fast on the NMR timescale. Additionally, three distinct signals occur between 26 and 27 ppm for $0.8 < \tau < 2.5$. The existence of MHL is practic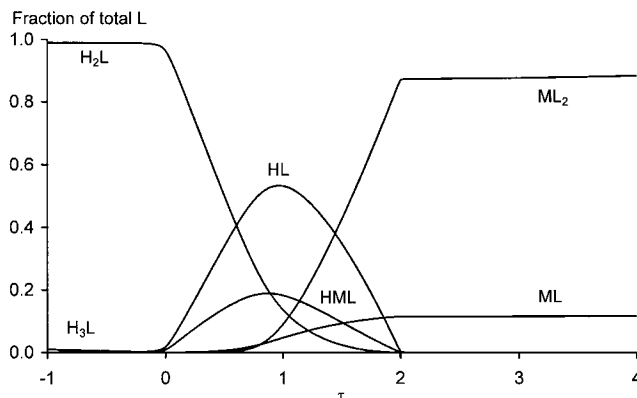ally restricted to this region (see the species distribution plot in Figure 7), but ML and ML_2 species exist until the end of titration ($\tau = 4$). However, these three additional signals observed are not consistent with such a simple model involving three types of complexes in rapid exchange with ligand ions H_iL^{i-2} ($i = 0–3$). They may indicate slow exchange or more likely the existence of further phosphorus-containing species, possibly representing polynuclear, oligomeric complexes. In the region of $1.5 < \tau < 3.2$, turbidity was also observed, but hitherto the formation of precipitates was not reported in the literature for this reaction. Further studies are suggested to understand and describe inhomogeneous systems.

β-Ala-P **2** and Mg^{2+} form labile complexes of type ML and MHL [7a,9]. This was deduced from potentiometric studies in aqueous solutions. But X-ray data suggest an octahedral outer-sphere structure in the solid phase, most simply described by $[Mg(H_2O)_6][H_2O\text{-}L]_2$, where the ammonium cationic site in L is not involved in coordination [11]. The NMR-controlled titration of **2** in the presence of
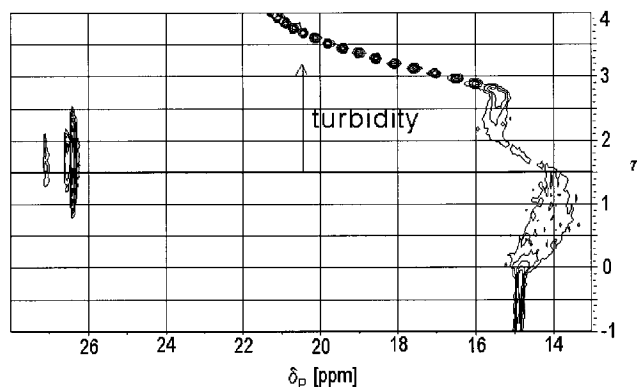
FIGURE 6 81 MHz $^{31}P\{^1H\}$-NMR-controlled titration of α-Ala-P **1** + Zn^{2+} (1:1) with NaOH. Prior to titration, 1 equivalent of HNO_3 was added to the titrand.

FIGURE 5 pH,δ curves, simulated with ABPLT. (A) **1** with NaOH, (B) **2** with NaOH, (C) **2** with TMAOH.


FIGURE 7 Distribution plot for the phosphor-containing species of α-Ala-P **1** and Zn^{2+} (1:1) as a function of titration grade τ.

Mg^{2+} [7a] is depicted in Figure 8. For $\tau > 1.4$ turbidity was observed. The MHL$^+$-species is formed in the region from $\tau = 0$ to $\tau = 1$, while the formation of ML is deduced from chemical shifts above $\tau = 1$. The ion-specific chemical shifts δ_P of 18.13 ppm and 20.34 ppm were calculated for MHL and ML, respectively.

*1-Aminoethane-1,2-bisphosphonic Acid (**3**).* This compound combines the structural elements of the parent molecules **1** and **2**. Based upon the experimental acidity constants (pK_1 = 1.28, pK_2 = 1.43, pK_3 = 5.24, pK_4 = 6.79, and pK_5 = 11.73) it is tempting to derive a dominant deprotonation sequence, which is also in accordance with the results of the ^{1}P{^{1}H}-NMR-controlled titration [7a,7f] (Figure 9).

This δ-τ correlation plot shows the characteristic
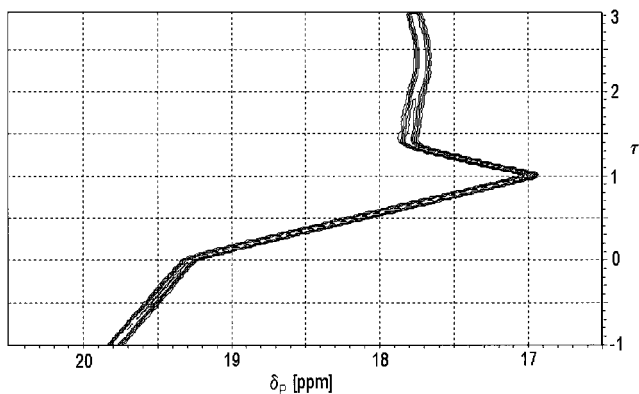
**FIGURE 8**   81 MHz ^{31}P{^{1}H}-NMR-controlled titration of β-Ala-P **2** + Mg^{2+} (1:1) with TMAOH. Prior to titration, 1 equivalent of HNO$_3$ was added to the titrand.
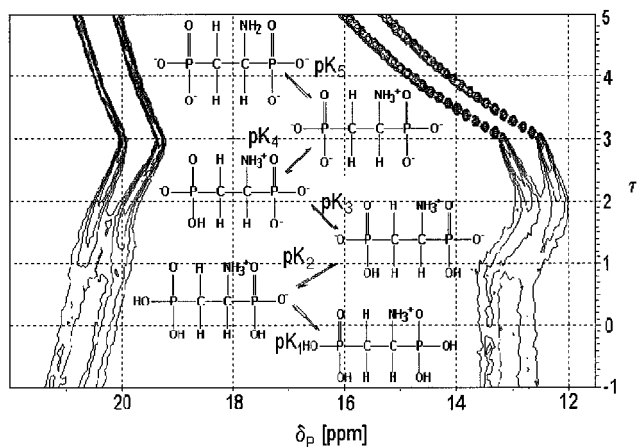

FIGURE 9   81 MHz ^{31}P{^{1}H}-NMR-controlled titration of Asp-P$_2$ **3** with NaOH. Prior to titration 1 equivalent of HNO$_3$ was added to the titrand.

doublet structure of an asymmetric P–C–C–P skeleton giving rise to a ^{31}P-AX-system with some AB-character. The minute second-order character is negligible with respect to the apparent transition frequencies. The low-field signal is attributed to the phosphonate unit, which is β to the amino function, while the high-field signal is attributed to the phosphonate at the α position. Between $-1.0 < \tau < 1.0$, the β signal is shifted upfield, while the α one is practically unchanged, indicating a deprotonation at the β-phosphonic acid group. In the region $1.0 < \tau < 2.0$, deprotonation takes place at the α-phosphonic acid group as indicated by a high-field shift for this group. For $2.0 < \tau < 3.0$, the final POH proton from the β-phosphonic acid group is abstracted resulting in a high-field shift. The parallel signal attributed to the α-phosphonic unit is shifted to low-field as a result of a remote neighboring group effect. Above $\tau = 3$, both signals are shifted down-field, which unequivocally indicates the deprotonation of the ammonium cationic group. This final deprotonation effect is stronger for the α- than for the β-phosphonate unit, which is consistent with observations made for the simple **1** and **2** compounds as shown in Figure 10.

The vicinal coupling constant, $^3J_{PP}$, is a sensitive function of τ or pH spanning a range from 40 to 57 Hz. For pH = 6.2, a minimum of $^3J_{PP}$ is observed corresponding to the formation of the species LH^{2-}. These findings are consistent with results from the analogous structure of H$_2$O$_3$P–CH(CH$_3$)–CH$_2$–PO$_3$H$_2$ [7h]. It is tempting to deduce that the P–C–C–P skeleton in LH$_2^{2-}$ is not strictly antiperiplanar but closer to a gauche conformation (see Figure 11).
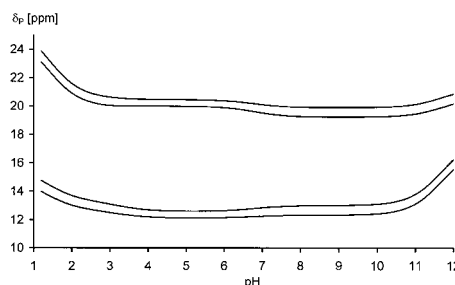
FIGURE 10   pH,δ diagram for the dynamic ^{31}P-AX-system of Asp-P$_2$ **3**, simulated with ASPPLT [5e]. Lower traces: α-P-doublet, upper traces: β-P-doublet.
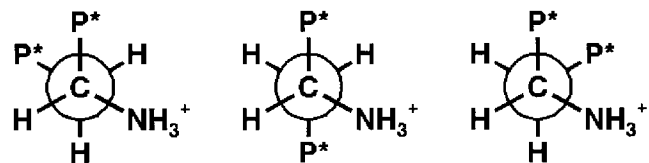
FIGURE 11   Three canonical rotamers of Asp-P$_2$ **3**.

The ion-specific NMR parameters are listed in Table 5.

$^{13}C\{^1H\}$-NMR Studies on Simple Aminophosphonates

Additional informations on aminophosphonic acids may be obtained using ^{13}C NMR techniques. Titration-dependent indicators are chemical shifts δ_C and the couplings constants $^nJ_{PC}$.

1-Aminoethanephosphonic Acid (1). ^{13}C-NMR spectroscopy proved to be a valuable tool for studying macroscopic and microscopic dissociation equilibria. Here we wish to demonstrate ^{13}C NMR-controlled titrations applied to the characterization of aminophosphonic acids. Figure 12 shows the $^{13}C\{^1H\}$-NMR-controlled titration of 1-aminophosphonic acid with NaOH [7a]. Similar to the ^{31}P case (see previous section), the first deprotonation step is not accompanied with a change in δ_C at titration degrees of $-1 < \tau < 0$. Within the range of $\tau = 0$ and $\tau = 1$, a typical low-field shift for C_1 and C_2 indicates the second deprotonation of the phosphonic acid unit, while for $\tau = 1$ to $\tau = 2$, the characteristic high-field shift for C_1 but a low-field shift for C_2 indicates the deprotonation of the NH_3^+ group. The ion-specific chemical shifts and coupling constants are given in Table 6.

2-Aminoethanephosphonic Acid (2). In contrast to the α-analogue **1**, deprotonations of POH and NH_3^+ groups lead to low-field shifts for both carbons C_1 and C_2 as shown in Figure 13 [7a]. The ion-specific chemical shifts and coupling constants, together with their gradients, are summarized in Table 6. It

is interesting to note that the one-bond coupling constant $^1J_{PC}$ is a nonmonotonous function of titration grade. Deprotonation of P–OH is connected with a decrease in $^1J_{PC}$, while ionization of the ammonium site gives rise to an increase in $^1J_{PC}$. Between $1 < \tau < 2$, deprotonation takes place on the ammonium cationic site, which is reflected in a low gradient for the adjacent C_1 of **1**, but a larger one for C_1 of **2**. Similar remote effects have been reported for aminocarboxylic acids as well [12].

Multinuclear NMR Studies on Modified Aminophosphonates

2,2,2-Trifluoro-1-aminoethanephosphonic Acid (4). $^{31}P\{^1H\}$-, $^{13}C\{^1H\}$- und ^{19}F NMR-controlled ti-
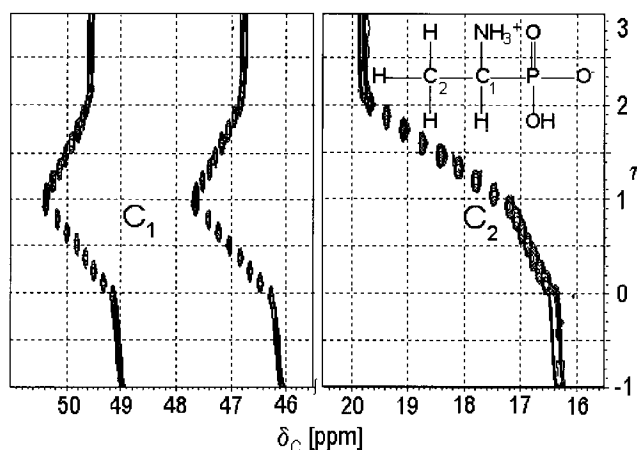
FIGURE 12 50.29 MHz $^{13}C\{^1H\}$-NMR-controlled titration of α-Ala-P **1** with NaOH. Prior to titration, 1 equivalent of HNO_3 was added to the titrand.

FIGURE 13 50.29 MHz $^{13}C\{^1H\}$-NMR-controlled titration of β-Ala-P **2** with NaOH. Prior to titration, 1 equivalent of HNO_3 was added to the titrand.

TABLE 5 Ion-Specific Chemical Shifts δ_P (ppm), Coupling Constants $^3J_{PP}$ (Hz) and Corresponding Gradients from 81 MHz $^{31}P\{^1H\}$-NMR-Controlled Titration of Asp-P$_2$ **3** with NaOH

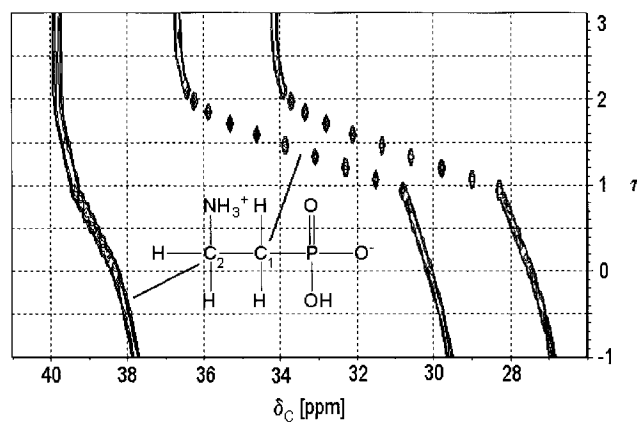| Species	$\delta_{P\alpha}$	$^3J_{PP}$	$\delta_{P\beta}$
H_4L	14.85	68.6	24.89
H_3L^-	13.00	52.0	20.29
H_2L^{2-}	12.36	37.7	20.23
HL^{3-}	12.67	54.4	19.56
L^{4-}	17.55	57.8	20.99
Gradients	$\delta_{P\alpha}$	$^3J_{PP}$	$\delta_{P\beta}$
4	1.85	16.6	4.60
3	0.64	14.3	0.06
2	−0.31	−14.7	0.67
1	−4.88	−3.3	−1.40

Note: Data for H_5L^+ were not iterated.

TABLE 6 Ion-Specific Chemical Shifts δ_C (ppm), Coupling Constants $^1J_{PC}$ [Hz] and their gradients Δ_i (ppm or Hz) from $^{13}C\{^1H\}$-NMR-controlled titration of α-Ala-P **1** and of β-Ala-P **2** with NaOH

| Species | α-Ala-P **1** | | | β-Ala-P **2** | | |
	δ_{C1}	$^1J_{PC}$	δ_{C2}	δ_{C1}	$^1J_{PC}$	δ_{C2}
H_3L^+	46.80	151.5	16.00	27.50	137.4	37.09
H_2L	47.70	143.8	16.43	28.73	131.4	38.22
HL^-	49.07	134.5	17.23	29.47	124.8	39.28
L^{2-}	48.15	138.0	19.79	35.45	126.5	39.76
Gradients	δ_C	$^1J_{PC}$	δ_{C2}	δ_{C1}	$^1J_{PC}$	δ_{C2}
Δ_1	0.90	-8.7	0.43	1.23	-6.0	1.13
Δ_2	1.37	9.3	0.80	0.74	-6.6	1.04
Δ_3	-0.92	3.5	2.55	5.98	1.3	0.47

*Note:*Iteration with SON4 [7a].

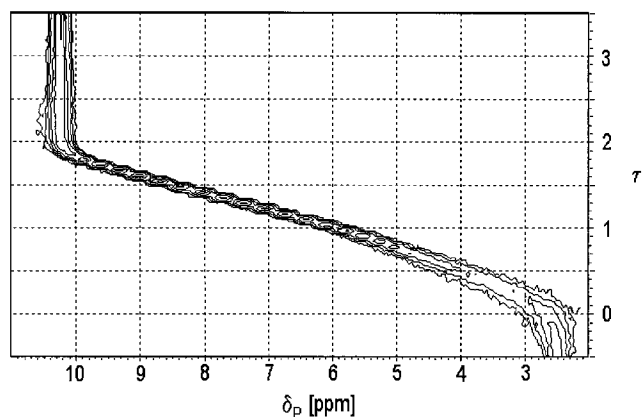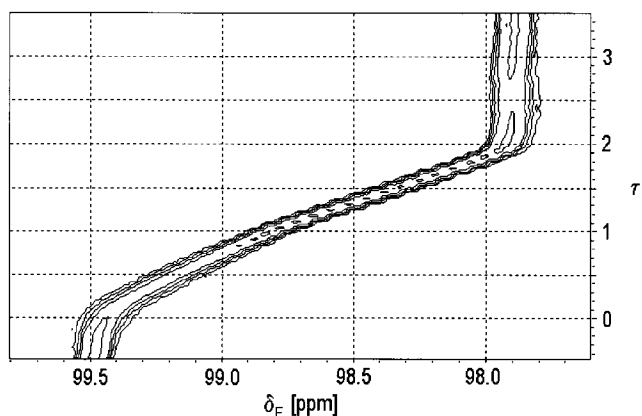**FIGURE 14** 81 MHz $^{31}P\{^1H\}$-NMR-controlled titration of F-α-Ala-P **4** with NaOH.

trations were used to study the trifluorinated compound **4** [6a,13,7a]. It is interesting to compare the response of ^{31}P and ^{19}F titration sensor nuclei in Figures 14 and 15.

From the first derivative curves $d\delta_P/dpH$ and $d\delta_F/dpH$ (not shown here), acidity constants were derived: $pK_3 = 6.60$, $pK_2 = 4.24$, and $pK_1 < 1$, which are consistent with the expected deprotonation sequence of $PO_3H_2 \rightarrow PO_3H^- \rightarrow PO_3^{2-}$ and finally $NH_3^+ \rightarrow NH_2$. It is worthwhile to remember the change of sign from the second deprotonation gradient, which is in contrast to observations made for the nonfluorinated analogue **1** shown previously. Strong electronegativity effects of the CF_3 group induce a negative gradient for the deprotonation of $PO_3H^- \rightarrow PO_3^{2-}$. This observation is not typical of phosphonic acids RPO_3H_2 but is consistent with the parent compound H_3PO_4. Ion-specific NMR data of the fluorinated **4** and nonfluorinated **1** are compared in Table 7.

CF_3-$CH(NH_2)$-PO_3H_2 differs remarkably from CH_3-$CH(NH_2)$-PO_3H_2. Deprotonation of $PO_3H^- \rightarrow PO_3^{2-}$ is connected with a low-field shift in δ_P of the fluorinated compound, while a high-field shift is significant for the nonfluorinated parent. A downfield shift in δ_P for $NH_3^+ \rightarrow NH_2$ is characteristic for CF_3-$CH(NH_2)$-PO_3H_2 and CH_3-$CH(NH_2)$-PO_3H_2 as well. The ^{19}F-NMR sensor on the trifluoromethyl group exhibits a high-field shift in δ_F for both deprotonation steps $PO_3H^- \rightarrow PO_3^{2-}$ and $NH_3^+ \rightarrow NH_2$ as well. The opposite holds for the chemical shifts δ_C of both carbon atoms C_1 and C_2 (not shown here).

(2-Aminoethyl)-methylphosphinic Acid (5).
This compound is the phosphinic acid analogue of

FIGURE 15 188 MHz ^{19}F-NMR-controlled titration of F-α-Ala-P **4** with NaOH.

TABLE 7 Ion-Specific Chemical Shifts δ_F and δ_P (ppm) from NMR-Controlled Titration of **4**

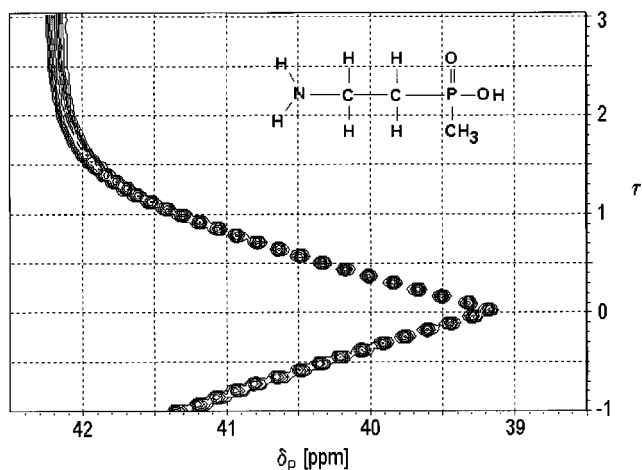| Species | F-α-Ala-P **4** | | α-Ala-P 1 |
	δ_F	δ_P	δ_P
H_3L^+	99.7[a]	2.0[a]	15.0[a]
H_2L	99.6	2.2	14.92
HL^+	98.8	5.9	13.08
L^{2-}	97.9	10.3	22.25
Gradients	δ_F	δ_P	δ_P
2	0.8	-3.7	1.84
1	0.9	-4.4	-9.17

[a]Not iterated value.

ciliatin **2**. The potentiometrically determined acidity constants are pK_1 = 2.0 and pK_2 = 10.04 [6b]. The first dissociation step can be assigned to the phosphinic acid moiety, followed by the deprotonation of the ammonium group. This behavior is nicely reflected in the ^{31}P{^{1}H}-NMR-controlled titration [7a], depicted in Figure 16. Titrating the hydrochloride of **5** with NaOH, the dissociation of the POH proton between τ = −1 and 0 is reflected by an upfield gradient (titration shift) of −2.5 ppm. A downfield gradient of comparable magnitude indicates the deprotonation at the remote NH$_3^+$ site.

*1-Aminopropanephosphonous Acid (**6**).* The values of the dissociation constants, pK_1 = 0.4 and pK_2 = 8.11, suggest the same deprotonation sequence for **6** as for **5** [7a]. However, the $\underline{\tau},\underline{\delta}$ representation (Figure 17) differs remarkably. Since the dissociation of the very acidic POH function is almost complete even at the start of the titration, no change can be observed in δ_P within a range spanning −1 < τ < 0. The unusually large low-field shift with a gradient of −12.5 ppm indicates the deprotonation of the NH$_3^+$ site. Because of the low abundance of species H$_2$L$^+$, only two ion-specific chemical shifts were evaluated in this case: δ_P(HL) = 20.83 ppm and δ_P(L$^-$) = 33.33 ppm.

ADVANCED TECHNIQUES: ACCURACIES OF OBSERVED AND CALCULATED PARAMETERS

A Case Study: 1-Hydroxyethane-1,1-Diphosphonic Acid (**7**)

A central aim of our investigations is to calculate ion-specific NMR parameters. As a more advanced treat-

ment, a novel error analysis has been introduced, which comprises all steps of the evaluation process. This method will be exemplified on our ^{31}P{^{1}H} stopped-flow NMR titration data set of HEDP **7**. This experiment is the very first one at 202 MHz ^{31}P measurement frequency on a high-field Bruker AVANCE 500 MHz spectrometer [8].
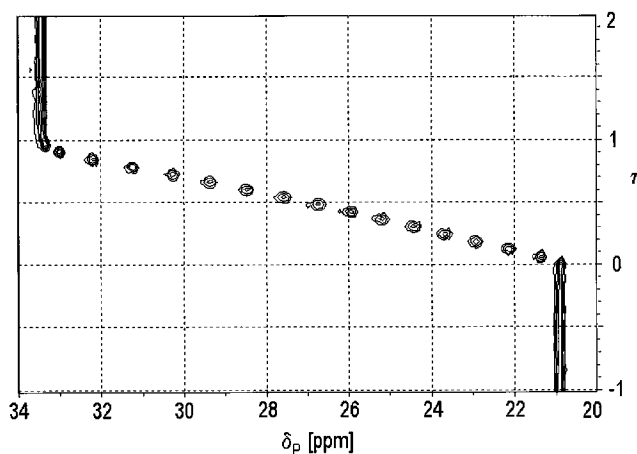
As a preliminary experiment, the glass electrode (model Schott N6280) has been calibrated in terms of hydrogen ion concentration by a blank titration: 30 mL 0.01 M HCl was titrated with 0.0975 M NaOH. To maintain almost constant ionic strength, the titrand contained 0.10 M NaCl as well. The resulting parameters of the extended Nernst equation,

$$E(\text{pH}) = E° + G \cdot \text{pH} + j_{H^+} \cdot 10^{-\text{pH}}$$
$$+ j_{OH^-} \cdot 10^{\text{pH} - \text{p}K_w} \qquad (23)$$

were calculated by linear regression: $E°$ = 402.87 ± 0.14 mV and G = −57.86 ± 0.02 mV/pH, whereas the diffusion potential coefficients j_{H^+} and j_{OH^-} were found to be negligible in the investigated region of 1.8 < pH < 11.7. These electrode calibration data were used afterwards to convert mV values to pH (pH denotes hereby −log c$_H$) from NMR-controlled titrations.

In the main experiment, 30 mL of titrand was used holding 0.01 M in HEDP, 0.01 M in HCl, and 0.10 M in NaCl. The titrator was added in 64 equidistant increments of 0.30 mL. For each titration volume, V_j, the potential difference of the glass electrode E_j has been recorded first, then the solution was pumped into the NMR probe head, and finally the jth FID was recorded and stored (see also the flowchart in Figure 2).

The analytical titration data set, $E_j(V_j)$ has been

FIGURE 16 81 MHz ^{31}P{^{1}H}-NMR-controlled titration of the AEP hydrochlorid **5** with NaOH. Prior to titration, 1 equivalent of HNO$_3$ was added to the titrand.

FIGURE 17 81 MHz ^{31}P{^{1}H}-NMR-controlled titration of APP″ **6** with NaOH. Prior to titration, 1 equivalent of HNO$_3$ was added to the titrand.

converted to its alternative representation $pH_j(\tau_j)$ using Equations 24 and 15, respectively. The pH versus τ curve is depicted in Figure 18. The formation constants of the four protolytic species $\beta(H_iL)$ have been iterated by the computer program ITERAX and are listed together with corresponding individual dissociation constants pK_i in Table 8.
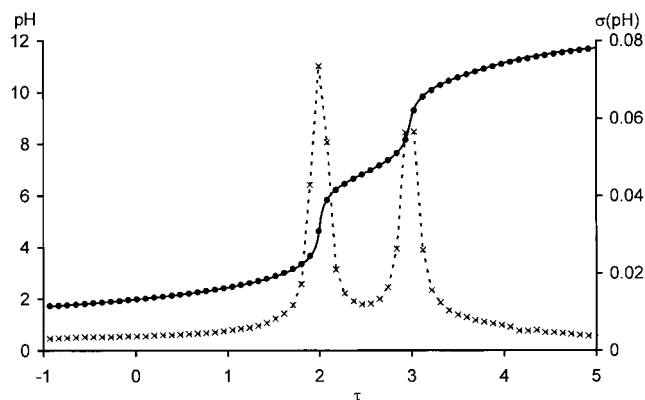
The error analysis [14,15] begins with the error estimation of the recorded pH values. To the rearranged Nernstian equation,

$$pH_j = \frac{E_j - E^\circ}{G} \qquad (24)$$

the Gaussian law of error propagation [16] has been applied, leading to the following expression:

$$\sigma^2(pH_j) = \left(\frac{\partial pH_j}{\partial E_j}\right)^2 \cdot \sigma^2(E_j) + \left(\frac{\partial pH_j}{\partial E^\circ}\right)^2 \cdot \sigma^2(E^\circ)$$
$$+ \left(\frac{\partial pH_j}{\partial G}\right)^2 \cdot \sigma^2(G) \qquad (25)$$

The estimated errors of the parameters E° and G have already been obtained in the electrode calibration session. On the other hand, the uncertainty of the measured potential difference $\sigma(E_j)$ changes with the progress of titration: it is smaller for well-buffered regions and larger close to inflection points. This fact can be quantitated by the following equation, which has been extensively used in computations of complex equilibria [4]:

$$\sigma^2(E_j) = \sigma_{exp}^2(E) + \left(\frac{\partial E}{\partial V}\right)_{|E = E_j}^2 \cdot \sigma_{exp}^2(V) \qquad (26)$$

where $\sigma_{exp}^2(E) \approx 0.1$ mV is the intrinsic uncertainty of the EMF measurements, determined in repeated experiments, and $\sigma_{exp}^2(V) \approx 0.02$ mL is the standard deviation of volume increments, based upon manufacturer specification. The first derivative of the titration curve has been generated numerically. Keeping all that in mind, the estimated uncertainty (standard deviation) of the jth pH value can be expressed as:

$$\sigma(pH_j) = \frac{\sqrt{\sigma_{exp}^2(E_j) + \left(\frac{\partial E}{\partial V}\right)_{|E = E_j}^2 \cdot \sigma_{exp}^2(V_j) + \sigma^2(E^\circ) + \sigma^2(G)/G^2}}{G}$$
$$\qquad (27)$$

Figure 18 clearly shows that the accuracy of pH values is largely governed by the contribution of the derivative term in Equation 27, describing the change in buffer capacity during the titration.

Now we are able to calculate the molar fractions and their corresponding standard deviations for an arbitrary pH. The general expression for the ith molar fraction χ_i in the general n basic case reads

$$\chi_i = \frac{[H_iL]}{[L] + [HL] + \dots + [H_nL]}$$
$$= \frac{\beta_i \cdot c_H^i}{\sum_{k=0}^{n} \beta_k \cdot c_H^k} = \frac{\beta_i \cdot c_H^i}{SUM} \qquad (28)$$

with the usual definition $\beta_0 \equiv 1$. Applying the law of error propagation to the above equation leads to:

$$\sigma^2(\chi_i) = \left(\frac{\partial \chi_i}{\partial \beta_i}\right)^2 \cdot \sigma^2(\beta_i) + \sum_{\substack{k=1 \\ k \neq i}}^{n} \left(\frac{\partial \chi_i}{\partial \beta_k}\right)^2$$
$$\cdot \sigma^2(\beta_k) + \left(\frac{\partial \chi_i}{\partial c_H}\right)^2 \cdot \sigma^2(c_H) \qquad (29)$$

After doing some algebra and substituting the variances of β and c_H with those of $\log \beta$ and pH, the standard deviation of the ith molar fraction is given by
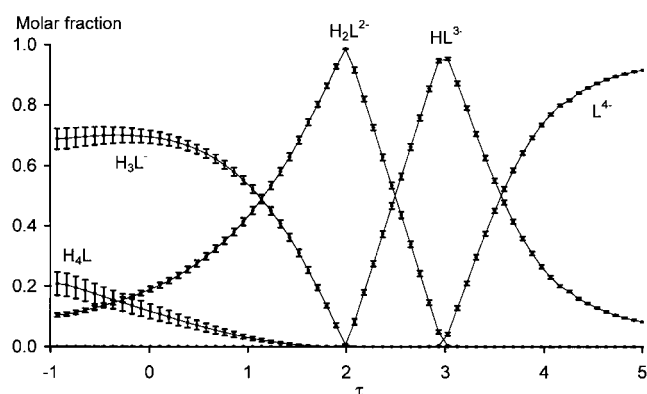
$$\sigma(\chi_i) = \frac{\beta_i c_H^i \cdot \ln 10}{SUM^2} \qquad (30)$$

$$\cdot \sqrt{(SUM - \beta_i c_H^i)^2 \cdot \sigma^2(\log \beta_i) + \sum_{\substack{k=1 \\ k \neq i}}^{n} [(\beta_k c_H^k)^2 \cdot \sigma^2(\log \beta_k)] + \left[i + \sum_{\substack{k=1 \\ k \neq i}}^{n} (\beta_k c_H^k(i - k))\right]^2 \cdot \sigma^2(pH)}$$

FIGURE 18   Titration curve pH with τ (symbol ●) of HEDP **7** with NaOH. The standard deviations of the pH values $\sigma(pH)$ (symbol x) have been calculated according to equation.

TABLE 8   Brutto Stability Constants and Acid Dissociation Constants of HEDP **7**, Calculated by ITERAX

log β(HL)	10.66 ± 0.01	pK_1	1.21 ± 0.12
log β(H$_2$L)	17.54 ± 0.01	pK_2	2.55 ± 0.03
log β(H$_3$L)	20.09 ± 0.02	pK_3	6.87 ± 0.02
log β(H$_4$L)	21.3 ± 0.1	pK_4	10.66 ± 0.01

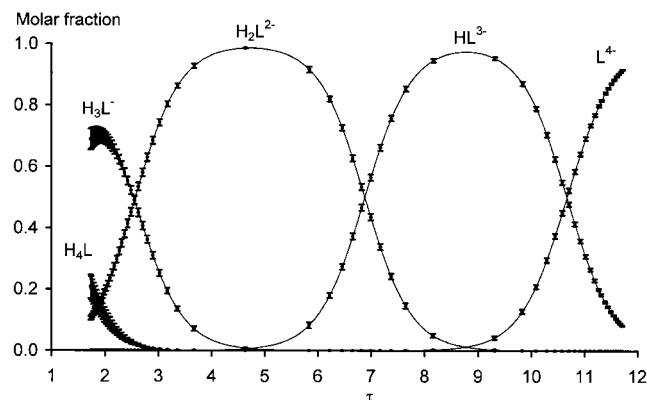*Note:* The uncertainties are standard deviations.

Using this expression the molar fraction curves with error bars was generated for the HEDP titration as a function of the degree of titration τ (Figure 19) or pH (Figure 20). The uncertainty decreases with increasing value of the molar fraction. At pH = 4.635, H_2L has a relative abundance of 0.986, with a corresponding relative error $\sigma(\chi)/\chi$ of 0.066%. However, at pH = 11.706 we found $\chi(H_2L) = 1.23 \cdot 10^{-6}$, connected with an increased relative error of $\sigma(\chi)/\chi =$ 2.84%. The relative uncertainties of 18% $< \sigma(\chi)/\chi <$ 46% for the abundance of the species H_4L are clearly consequences of the large error in the corresponding formation constant.

The next step is the critical evaluation of recorded NMR spectra. In Figure 21 the contour plot of the titration is depicted.

Maximum and minimum chemical shifts observed differ by 0.7 ppm only, a minor dissociation effect, which is found to be characteristic for geminal bisphosphonates (see also pamidronate **8**). Moreover, the half width of the peaks shows an abrupt change at the diprotonated species H_2L^{2-},

holding one proton on each phosphonate group (Figures 19 and 22). It is tempting to assume that formation of bridges like P–O–H–O–P or P–O–M–O–P (M alkali metal) is affiliated with this striking effect, but further investigations are needed for deeper understanding.

Summing up, the exact evaluation of the ion specific chemical shifts of this compound is a rather challenging task, which has been accomplished using three different, home-written programs. The three algorithms are briefly described and compared below.

Calculation of Ion Specific Chemical Shifts. Consider an n-basic acid H_nL with $nsp = n + 1$ protolytic species H_iL in solution, titrated stepwise in m experiments. Denoting the measured chemical shift for each jth observation $\langle \delta_j \rangle$ by b_j, the molar fraction of species $H_{i-1}L$ by a_{ji} and the unknown ion specific

FIGURE 19 Species distribution plot including error bars as a function of degree of titration τ for HEDP **7**.

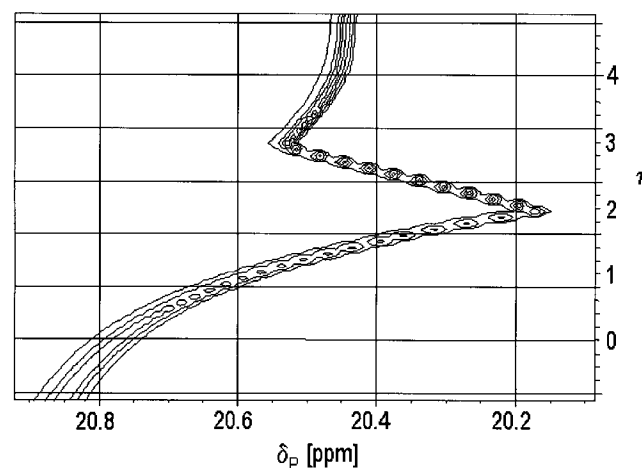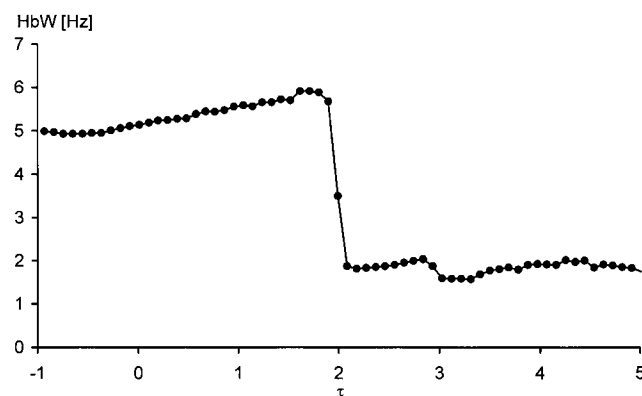**FIGURE 21** 202 MHz $^{31}P\{^1H\}$-NMR controlled titration of HEDP **7** with NaOH.

FIGURE 20 Species distribution plot including errors limits as a function of pH for HEDP **7**.

FIGURE 22 Change of ^{31}P NMR peak half widths in the titration of HEDP **7** with NaOH.

chemical shift of this species by δ_{i-1} leads to the jth member of a set of linear equations:

$$a_{j1}x_1 + a_{j2}x_2 + a_{j3}x_3 + ... + a_{j,nsp}x_{nsp} = \sum_{k=1}^{nsp}$$

$$a_{jk}x_k = b_j \quad j = 1, 2, ..., m \tag{31}$$

conveniently written in matrix notation as:

$$\mathbf{A} \cdot \mathbf{x} = \mathbf{b} \tag{32}$$

according to theory, $m = nsp$ measurements are needed to solve this system of linear equations uniquely:

$$\mathbf{x} = (\mathbf{A}^{-1} \cdot \mathbf{A}) \cdot \mathbf{x} = \mathbf{A}^{-1} \cdot \mathbf{b} \tag{33}$$

This simplest analysis gives only the ion-specific chemical shifts, but not their error estimations.

Multivariate Linear Regression. In practice, the number of experiments m exceeds that of unknown parameters nsp considerably. In addition, the experimental **b** vector contains random experimental error. The sum of squared deviations can be minimized in the least-squares treatment:

$$U = \sum_{j=1}^{m}(b_j^{exp} - b_j^{calc})^2 = \sum_{j=1}^{m}\left(b_j^{exp} - \sum_{k=1}^{nsp} a_{jk} \cdot x_k\right)^2$$

$$= (\mathbf{b} - \mathbf{A}\cdot\mathbf{x})^T(\mathbf{b} - \mathbf{A}\cdot\mathbf{x}) \to min! \tag{34}$$

Here each observed $\langle\delta_j\rangle$ value contributes with identical weight to the sum of error squares. This minimization yields in one step the best values of unknown parameters:

$$\mathbf{x} = (\mathbf{A}^T \cdot \mathbf{A})^{-1} \cdot (\mathbf{A}^T \cdot \mathbf{b}) \tag{35}$$

as well as their estimated standard deviations and the root mean square (rms) value of the fit. This method is used in our program AMPLSQ9 [7a] and in most programs in the literature as well [17].

Weighted Multivariate Linear Regression. A more sophisticated treatment [14] takes into account that the individual inaccuracy (standard deviation) of the observed chemical shifts changes significantly in the course of the titration (see in Figure 22). This standard deviation can be defined as a spectral halfwidth given in chemical shift units (ppm):

$$\sigma(\langle\delta\rangle) = \frac{\Delta v_{1/2}}{v_{\text{Spectrometer}}} \tag{36}$$

Consequently, a simple weighting scheme is introduced for each experimental point j,

$$w_j = \frac{1}{\sigma^2(\langle\delta_j\rangle)} \tag{37}$$

and used in the weighted least-square error function:

$$U_w = \sum_{j=1}^{m} w_j \left(b_j^{exp} - \sum_{k=1}^{nsp} a_{jk} \cdot x_k\right)^2$$

$$= (\mathbf{b} - \mathbf{A}\cdot\mathbf{x})^T \cdot \mathbf{W} \cdot (\mathbf{b} - \mathbf{A}\cdot\mathbf{x}) \to min! \tag{38}$$

Thus experiments bearing larger inaccuracies will exert a lesser influence upon the total sum of error squares, leading effectively to more realistic estimates of the **x** parameters:

$$\hat{\mathbf{x}} = (\mathbf{A}^T \cdot \mathbf{W} \cdot \mathbf{A})^{-1} \cdot (\mathbf{A}^T \cdot \mathbf{W} \cdot \mathbf{b}) \tag{39}$$

and their standard deviations.

Implicit Regression. The most complicated statistical tool [14], which we applied for the first time to this problem, takes into account that the molar fractions (a_{ji}) also contain specific errors, as derived in Equation 30. Strictly speaking, this fact hampers the application of the classical least-squares methods previously described, where error-free independent variables are assumed. In the implicit regression, the difference of independent and dependent variables ceases, leading to the following, composite error function:

$$U_{impl} = \sum_{j=1}^{m}\left[\sum_{i=1}^{nsp} \frac{(a_{ji}^{exp} - a_{ji}^{calc})^2}{\sigma^2(a_{ji}^{exp})} + \frac{(b_j^{exp} - b_j^{calc})^2}{\sigma^2(b_j^{exp})}\right] \tag{40}$$

Besides minimizing this function, the linear set of Equation 31 must be fulfilled as well. We solved this constrained extremum problem using the Deming algorithm [18]; the mathematical details will be discussed elsewhere [14]. This method finally leads to the maximum likelihood estimates of the parameters wanted, to corresponding estimated standard deviations and to the global rms value as well.

Results for **7** obtained by these three different evaluation methods are compared in Table 9. The implicit regression method, with a more rigid error treatment leads to higher and more realistic error estimates for the individual parameters.

For all the methods, more accurate values for the chemical shifts are obtained for the species L^{4-}, HL^{3-}, and H_2L^{2-} with high abundance, while larger errors are connected with the less populated species. Particular attention should be paid toward the unusually large error in $\delta(H_4L)$ as calculated by the implicit regression technique. This is dominantly a result of large errors in molar fraction of H_4L (see in Figure 20), not of the inaccuracy of the NMR measurement.

Pamidronic Acid (**8**)

Geminal bisphosphonic acids involving ω-amino-functions have attracted considerable interest in medicinal [19,20] and technical chemistry. In addition,

TABLE 9 Ion-Specific ^{31}P Chemical Shifts of HEDP **7**, Obtained with Different Evaluation Methods

Ion-Specific Chemical Shift (ppm)	Linear Regression	Weighted Linear Regression	Implicit Regression
$\delta_{L^{4-}}$	20.4346 ± 0.0007	20.4345 ± 0.0004	20.4346 ± 0.0285
$\delta_{HL^{3-}}$	20.5336 ± 0.0009	20.5342 ± 0.0004	20.5342 ± 0.0773
$\delta_{H_2L^{2-}}$	20.1693 ± 0.0009	20.1663 ± 0.0006	20.1653 ± 0.0407
$\delta_{H_3L^{-}}$	20.8806 ± 0.0018	20.8835 ± 0.0023	20.8916 ± 0.3272
δ_{H_4L}	21.0828 ± 0.0091	21.0731 ± 0.0118	21.0209 ± 2.4562

Note: Uncertainties are estimated standard deviations.
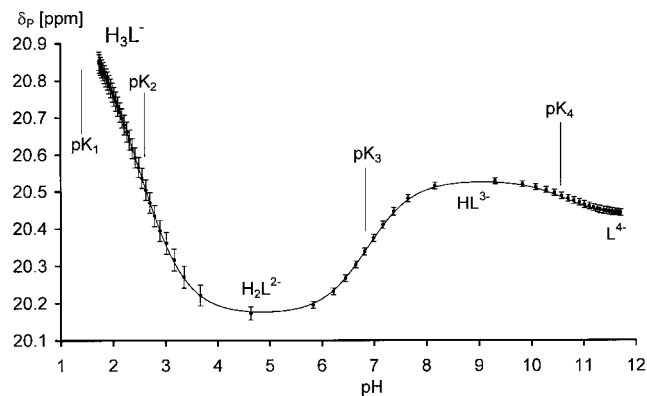
FIGURE 23 Experimental NMR titration curve pH-δ_P of HEDP **7** together with the fitted function. The error bars represent the contributions the NMR half widths.

TABLE 10 Acidity Constants of Geminal Bisphosphonic Acids: HEDP **7**, pamidronate **8**, and alendronate **9**

|	8	9	7
pK_1	1.24	1.33	1.21
pK_2	1.93	2.22	2.55
pK_3	6.04	6.39	6.87
pK_4	10.18	10.96	10.66
pK_5	12.14	11.82	–

TABLE 11 Dissociation Constants, Ion-Specific ^{31}P Chemical Shift δ_{H_iL} and Gradients Δ_i (ppm) from 81 MHz ^{31}P{^{1}H}-NMR-Controlled Titration of Pamidronate **8**

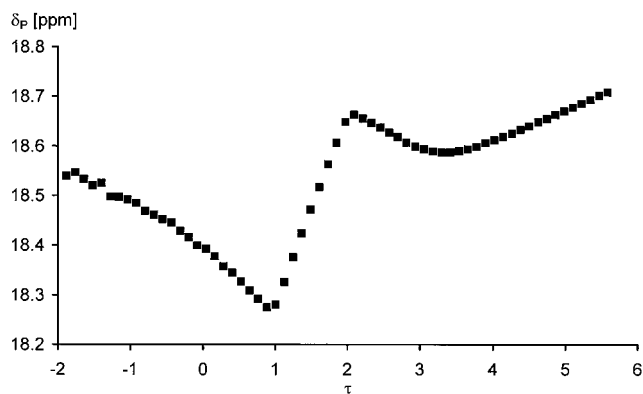| H_iL^{1-4}	δ_{H_iL}
5	18.93
4	18.72
3	18.27
2	18.68
1	18.55
0	18.82

Gradients	Δ_i
5	0.21
4	0.45
3	-0.41
2	0.13
1	-0.27

analytical and structural investigations are accessible in the literature [21–23]. We have characterized pamidronic acid **8** and alendronic acid **9** by potentiometric and by 81 MHz ^{31}P{^{1}H}-NMR-controlled titration using the BRUKER 200 AVANCE spectrometer [15]. Since pamidronic acid is less soluble in the acidic range than HEDP **7**, a retro-titration was performed: the compound was dissolved in 6 equivalents of NaOH and titrated back in 64 steps with HCl until an excess of 2 equiv. HCl was achieved. Dissociation constants and ion-specific chemical shifts with errors are given in Table 10. Titration diagrams are shown in Figures 24–27.

We have no evidence for a deprotonation of the carbinol proton in aqueous solution. Introducing the ammonium function into an HEDP-analogue skeleton increases the pK values of all the POH groups. Increasing distance between the bisphosphonate and ammonium units (pamidronate **8** → alendronate **9**) leads to a significant increase in pK_1 to pK_4. The last acidity constant, pK_5, assigned to the NH$_3^+$ → NH$_2$ deprotonation exhibits, however, the opposite trend, indicating the increasing acidity-modifying (inductive) interaction of bisphosphonate and amino sites with their decreasing covalent distance.

A diagram including the molar fractions together with their calculated errors (using Equation 30) for pamidronic acid is depicted in Figure 24.
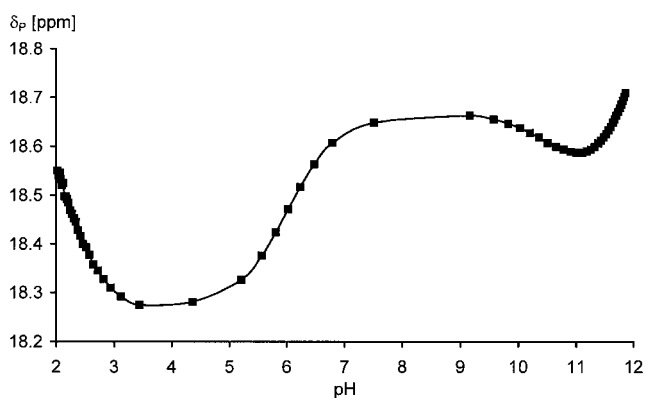
A novel, attractive graphical representation is given in Figure 28: the τ,δ stacked plot shows the retro-titration of pamidronate. Characteristic changes in chemical shifts and spectral half widths are clearly visible as functions of the degree of titration. Species H$_3$L, H$_2$L, HL, and L have sharper lines (around 2 Hz), while the introduction of additional protons gives rise to a very strong increase in spectral half widths HWB (up to 11 Hz). This phenome-
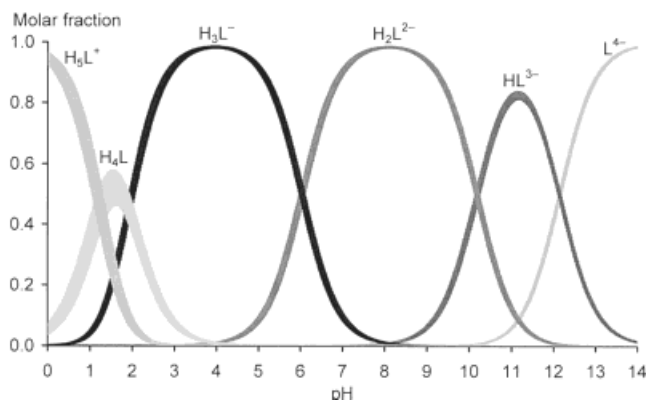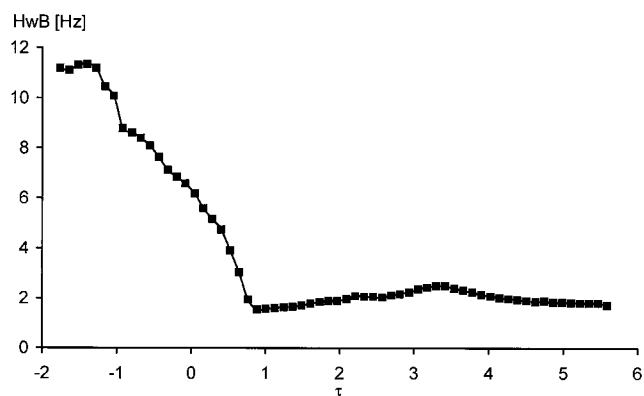
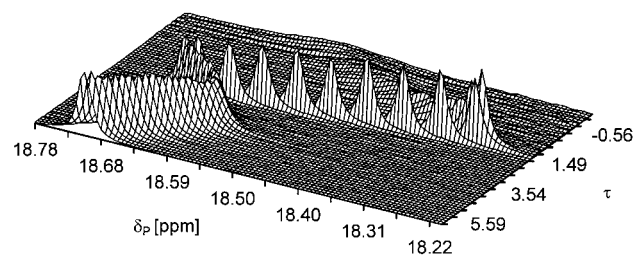**FIGURE 24** Species distribution diagram with error bars for pamidronate **8**.

FIGURE 27 Spectral half widths HWB [Hz] of **8** as a function of the degree of titration τ.

FIGURE 25 The chemical shift δ_P of pamidronate **8** as a function of the degree of titration τ.

FIGURE 28 τ,δ stacked plot for a 81 MHz $^{31}P\{^1H\}$ NMR-controlled titration of pamidronate **8**.

non corresponds to observations made for HEDP **7** discussed previously.

INVESTIGATION OF MICROSCOPIC DISSOCIATION EQUILIBRIA

Consider the two-step dissociation of a dibasic acid H_2L (charges omitted), with groups noted by 1 and 2 in Figure 29. For first-order acids, the dissociation occurs in well-separated pH regions: $pK_2 - pK_1 > 3$, and hence the macroscopic pK values characterize the acidity of the individual moieties. If, however, the acidities are comparable (second-order acids), a kind of isomerism with respect to site of protonation arises: the monoprotonated species HL exists in the solution in the form of two microspecies: in particle BA group 1 is ionized, while in AB group 2 is anionic.

The formation of microspecies can be described in terms of microscopic dissociation constants (k_i, frequently reported as pk_i), analogous to the macroscopic ones. The relationships between macro- und microconstants are

$$K_1 = k_1 + k_2 \tag{41}$$
$$K_2^{-1} = k_3^{-1} + k_4^{-1} \tag{42}$$
$$K_1 \cdot K_2 = k_1 \cdot k_3 = k_2 \cdot k_4 \tag{43}$$

FIGURE 26 The chemical shift δ_P of pamidronate **8** as a function of pH.

With the aid of microconstants, the site-specific degrees of dissociation (deprotonation fraction curves) of groups 1 and 2 can be derived:

$$\alpha_1([H^+]) = \frac{[BA] + [BB]}{[AA] + [AB] + [BA] + [BB]}$$

$$= \frac{k_1 \cdot [H^+] + k_2 k_4 \cdot [H^+]^2}{1 + (k_1 + k_2) \cdot [H^+] + k_2 k_4 \cdot [H^+]^2} \quad (44)$$

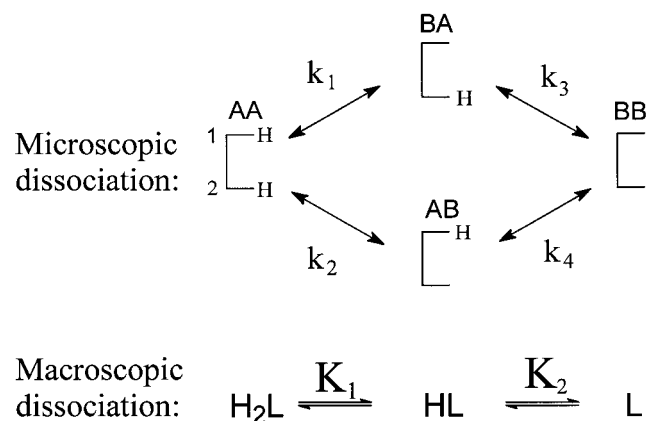$$\alpha_2([H^+]) = \frac{[AB] + [BB]}{[AA] + [AB] + [BA] + [BB]}$$

$$= \frac{k_2 \cdot [H^+] + k_2 k_4 \cdot [H^+]^2}{1 + (k_1 + k_2) \cdot [H^+] + k_2 k_4 \cdot [H^+]^2} \quad (45)$$

α_1 shows for any pH, which fraction of groups 1 are ionized at that pH. α_2 has a similar meaning for site 2. The α(pH) curves have a sigmoid shape, and microconstants can be obtained by nonlinear regression (shown subsequently).

Generalization of microdissociation equilibrium theory to the n-basic case can be found in the literature [7b,24,25].

Because of their continuous interconversion, microspecies are analytically inseparable and give rise to common spectroscopical signals. Accordingly, the calculation of microconstants always demands a priori assumptions of chemical nature. In the hyphenated technique UV spectroscopy-potentiometry, the standard assumption is that in a spectral interval only one chromophore absorbs [26a,27], thus reflecting the dissociation status of one functional group selectively (see example B below). In NMR spectroscopy, sensor nuclei (for instance, nonlabile protons in the vicinity of the functional groups) are assumed to monitor the site-specific ionization [7f,28].

Microscopic acid-base and complex formation [28] processes are significant primarily in pharmaceutical [29], biomedical [30,31], and physical organic chemistry [32].

Here we present two examples of microequilibria, investigated by pH-dependent NMR spectroscopy. First, **10** will be discussed as a first-order case, where one protonation pathway overwhelmingly dominates the alternative one. The second case is the UV-pH study of **11**. Finally, results on the microdissociation of **13** are reported, where the microspecies AB and BA are almost equipopulated.

### Limiting Case A: (N-ethyl-aminomethyl)-Methylphosphinic Acid (*10*)

The macroscopic dissociation constants of this compound have been determined as pK_1 = 0.99 and pK_2 = 8.91 [6c]. Owing to the great difference in their acidity, these constants can be readily assigned to the phosphinic acid and ammonium groups denoted by 1 and 2, respectively, in Figure 29. In other words, dissociation occur almost exclusively via the protonation pathway with the zwitterionic microspecies BA (see Figure 29). Consequently, the corresponding microconstants follow: p$k_1 \approx$ pK_1 and p$k_3 \approx$ pK_2.

A probe, acidified by 1 equivalent of HNO_3 to increase the population of H_2L^+ ($\tau = -1$) was titrated with NaOH, monitored by ^{13}C{^{1}H}-NMR [7a]. The resulting δ-τ plots in Figures 30 and 31 show that C_4 selectively reflects the ammonium-deprotonation between $\tau = 0$ and $\tau = 1$. C_1 monitors the ionization of both sites, similar to the case of 1-aminoethanphosphonic acid. An interesting long-range effect can be observed for the titration behavior of C_3 in Figure 30: the dissociation of the remote ammonium site is also reflected, but with an upfield shift. Similar phenomena have been reported for aminocarbonic acids [12].

Although C_4 is a selective indicator nucleus for

FIGURE 29 Microscopic and macroscopic dissociation schemata of a dibasic acid.
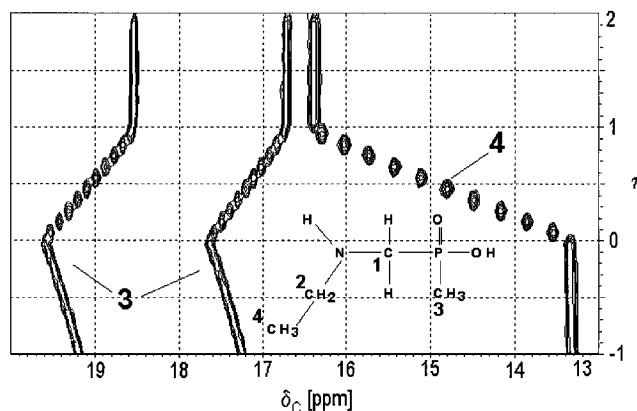
FIGURE 30 50.29 MHz ^{13}C{^{1}H}-NMR controlled titration of EAMP′ **10** with NaOH. Expansion of the methyl spectral region.
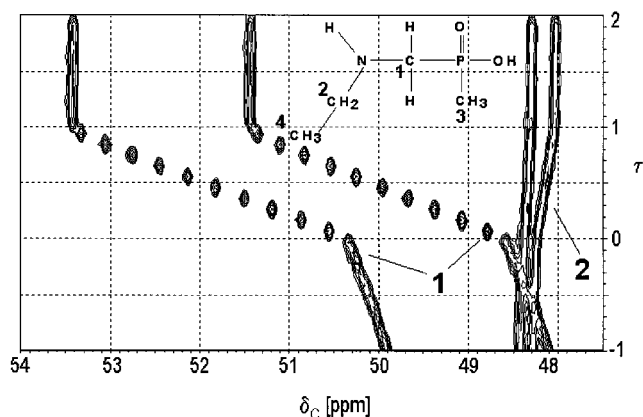
FIGURE 31 50.29 MHz ^{13}C{^{1}H}-NMR controlled titration of EAMP′ **10** with NaOH. Expansion of the methylene spectral region.

FIGURE 32 81 MHz ^{31}P{^{1}H}-NMR controlled titration of APHP **11** with HCl. Prior to titration, 2.4 equivalents of TMAOH were added.
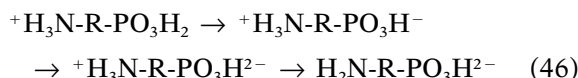
the amine site, the concentration of the neutral microspecies AB is so low that the microconstants for the minor protonation pathway, pk_2 and pk_4, cannot be determined precisely from this experiment.

4-Aminophenylphosphonic Acid (**11**)

It is interesting to compare the deprotonation sequences of aliphatic and aromatic aminophosphonic acids. As a pair of model compounds, 3-aminopropane phosphonic acid **12** and 4-aminophenylphosphonic acid **11** were chosen, and ^{31}P{^{1}H}-NMR controlled titrations were performed [7a]. Since the aromatic ligand is less soluble in water, a retro-titration was required: the acid was dissolved in aqueous TMAOH solution and titrated with HCl (Figure 32). The resulting ion-specific chemical shifts are listed in Table 12.
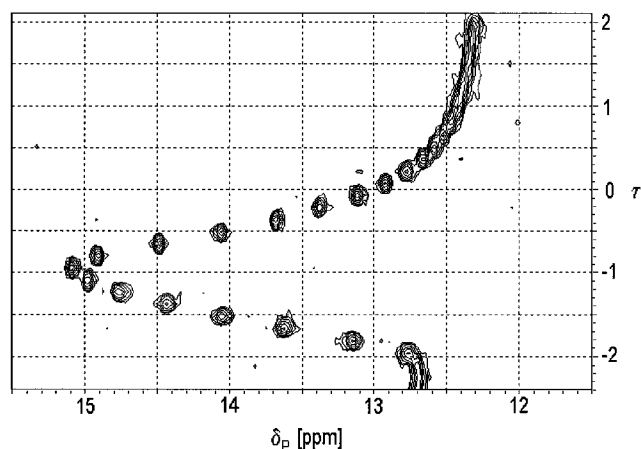
Looking into the gradients, it is immediately clear that the dominant deprotonation sequences must be different for the two compounds: gradient Δ_1 is negative for **11** but positive for the aliphatic **12**. The opposite is true, however, for the gradient Δ_2. The deprotonation on POH is always indicated by a negative gradient while that on NH$_3^+$ is connected with a positive one.

From these results, the following deprotonation sequence can be deduced for **12**

$$^+H_3N\text{-}R\text{-}PO_3H_2 \rightarrow {}^+H_3N\text{-}R\text{-}PO_3H^-$$
$$\rightarrow {}^+H_3N\text{-}R\text{-}PO_3H^{2-} \rightarrow H_2N\text{-}R\text{-}PO_3H^{2-} \quad (46)$$

while the complete ionization scheme of **11** is represented in Figure 33.

Additional UV-vis-controlled titrations using the hard- and software concept of PHOTO__T [26b,26c,26a] showed that **11** is in fact involved in a
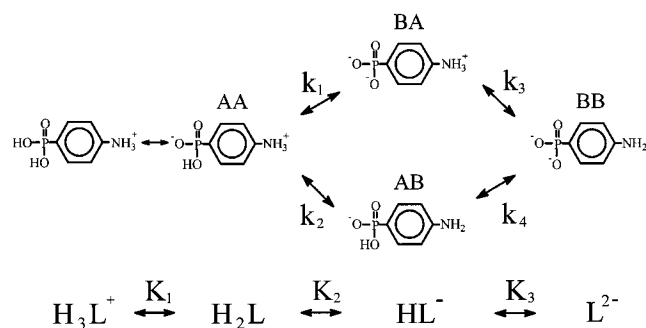
TABLE 12 Ion-Specific ^{31}P Chemical Shifts δ_{H_iL} and Gradients Δ_i (ppm) for Compounds **11** and **12**

Compound Species H$_i$L	**11** δ_{H_iL}	**12** δ_{H_iL}
H$_3$L$^+$	~13	n.d.
H$_2$L	12.16	24.48
HL$^-$	15.29	21.28
L^{2-}	12.7	22.87
Gradients	Δ_i	Δ_i
2	−3.13	2.20
1	2.59	−1.59

Note: Iteration with SON4; n.d., not determined.

FIGURE 33 Complete ionization scheme of APHP **11**.

microscopic dissociation equilibrium following Figure 33.

The absorption at 292 nm is assumed to reflect the deprotonation at the amino site selectively. From this site-specific spectroscopic titration curve, the microconstants were iterated by PHOTO__T and

listed in Table 13 [26a]. The species distribution curves in Figure 34 show that the macroscopic species HL$^-$ at pH = 6 is represented by ca. 90% of $^+$H$_2$N-R-PO$_3$H$^-$ (BA) and 10% of $^+$H$_3$N-R-PO$_3^{2-}$ (AB) [26a].

The protonation sequence found is consistent with UV-vis-controlled titrations of the simplified model compounds, aniline hydrochloride and phenylphosphonic acid [26a].

In principle, ^{13}C{^{1}H}-NMR-controlled titration may lead to a similar solution when monitoring the aromatic C$_1$ and C$_4$ carbons, but the low solubility of the model compound has prevented the corresponding experiments up to now.
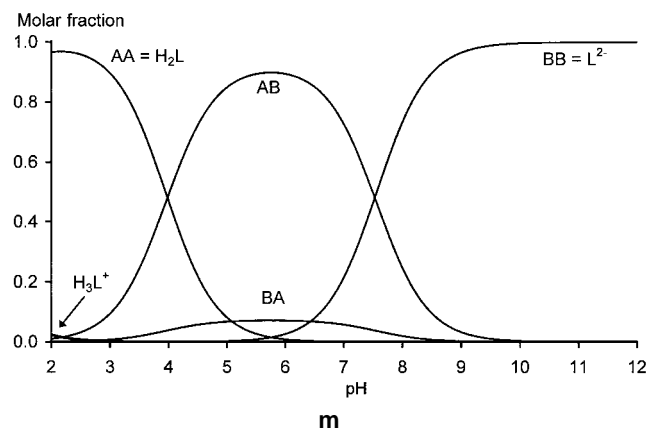
Limiting Case B: Glufosinate (13)

This γ-phosphinic analogue of glutamic acid is a natural compound, isolated from two species of *Streptomyces* fungi. It is produced on the industrial scale as well, and its ammonium salt is used as a broad-spectrum contact herbicide. Glufosinate inhibits glutamine synthetase, a key enzyme in the synthesis of glutamine. Inhibition of this enzyme gives rise to an increase of a number of toxic materials, such as ammonia in the cell, and the plant dies within a few days [33].

The macroscopic dissociation behavior of the molecule has been studied by potentiometric titra-

tions [14]. The most basic pK value of the molecule, pK_3 = 9.42, characterizes the acidity of the ammonium group. The other two values, pK_2 = 2.69 and pK_1 = 1.7 quantitate the overlapping dissociation of the carboxylic and phosphinic groups, but they cannot be directly assigned to these individual sites. The carboxylic function denoted by (1) and the phosphinic acid site (2), the protonation scheme on Figure 35 shows their overlapping equilibria at a submolecular level. (The protonation state of the amino group remains unaltered at pH < 6, thus glufosinate can be treated as a dibasic acid H$_2$L in this range.) The methylprotons are assumed to indicate selectively the phosphinic acid deprotonation, while the α-proton is supposed to indicate the dissociation state of the carboxyl moiety only. The NMR titration curves of these two nuclei, for this case obtained from a series of single NMR samples [14], are shown in Figure 36. The titration medium was 90% H$_2$O/ 10% D$_2$O. The total ionic strength of each sample was accurately adjusted to 1 M by addition of NaNO$_3$.

In the pH range between 7 and 11, the titration curve for the CH$_3$ group only indicates a minor titration shift of 0.03 ppm, in contrast to the 0.53 ppm

TABLE 13 Microscopic Dissociation Constants of APHP **11**, determined by UV titration [26a]

Microscopic Dissociation Constants

	NH$_3^+$		PO$_3$H$^-$
pk_1	5.08 ± 0.069	pk_2	3.98 ± 0.005
pk_4	7.53 ± 0.005	pk_3	6.43 ± 0.069
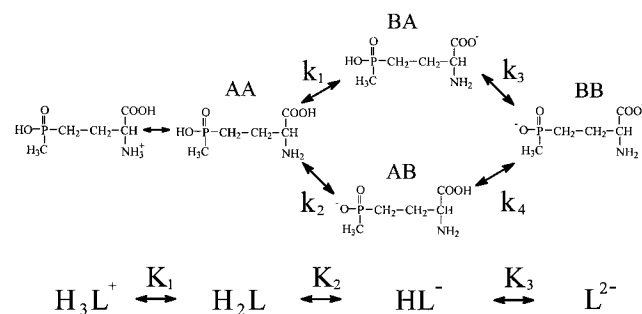
FIGURE 35   Complete ionization scheme of glufosinate **13**.

FIGURE 34   Species distribution curves for APHP **11**.
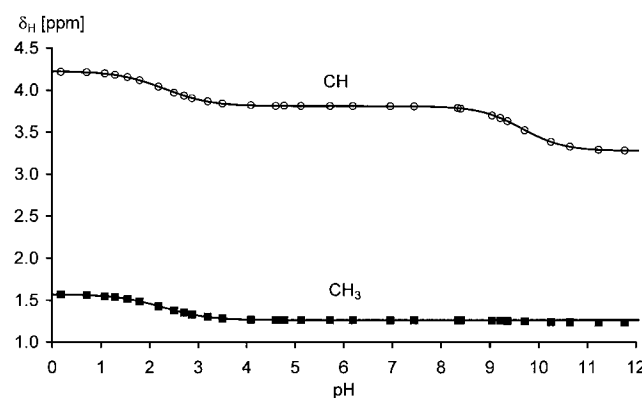
FIGURE 36   200 MHz ^{1}H NMR–pH titration curves of selected protons of glufosinate **13**.

deprotonation shift at the proximate CH proton. That indicates that inductive effects, accompanying deprotonations at α-functional groups, hardly influence the chemical shift of the constitutionally remote methylprotons. Thus the initial assumption of selectivity for the methyl sensor is supported.

The microconstants were calculated from experimental data $\langle\delta\rangle$ below pH 6 as follows. From the total of four microconstants, three are independent only and the fourth one is redundant, according to Equations 41–43 [7b,25]. Knowing the terminal ion-specific chemical shifts for the diprotonated and nonprotonated species, $\delta_{H_2L}^{CH_3} = 4.226 \pm 0.006$ ppm, $\delta_{H_2L}^{CH} = 1.573 \pm 0.006$ ppm, $\delta_L^{CH_3} = 3.812 \pm 0.004$ ppm, and $\delta_L^{CH} = 1.263 \pm 0.004$ ppm, it is possible to calculate the combined molar fractions (α_1 and α_2) for the carboxylic (1) and phosphinic acid (2) moieties:

$$\alpha_1 = \frac{\langle\delta^{CH}\rangle - \delta_L^{CH}}{\delta_{H_2L}^{CH} - \delta_L^{CH}}$$
$$= \frac{k_1 \cdot [H^+] + k_2 k_4 \cdot [H^+]^2}{1 + (k_1 + k_2) \cdot [H^+] + k_2 k_4 \cdot [H^+]^2} \quad (47)$$

$$\alpha_2 = \frac{\langle\delta^{CH_3}\rangle - \delta_L^{CH_3}}{\delta_{H_2L}^{CH_3} - \delta_L^{CH_3}}$$
$$= \frac{k_2 \cdot [H^+] + k_2 k_4 \cdot [H^+]^2}{1 + (k_1 + k_2) \cdot [H^+] + k_2 k_4 \cdot [H^+]^2} \quad (48)$$
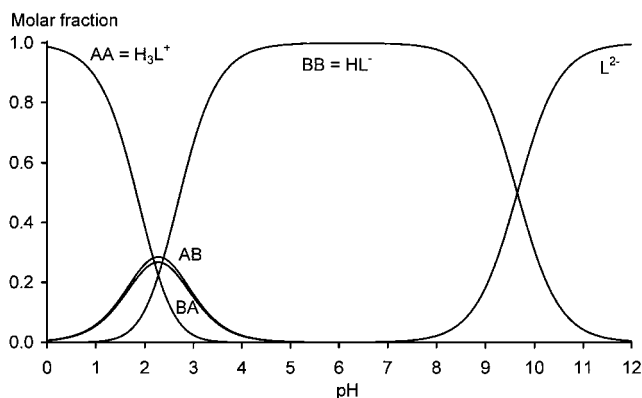

FIGURE 37 Species distribution curves of glufosinate **13**.

TABLE 14 Microscopic Dissociation Constants of Glufosinate **13**, Determined by ^{1}H NMR Titration

Microscopic Dissociation Constants

	COOH		$P(CH_3)(O)OH$
pk_1	2.20 ± 0.01	pk_2	2.17 ± 0.01
pk_4	2.385 ± 0.008	pk_3	2.357 ± 0.009

The three unknown microconstants were obtained by simultaneous fitting of Equations 47 and 48 to the experimental α(pH) data (see Figure 36).

The resulting microconstants (given as pK_i) are listed in Table 14. The acidity of the phosphinic acid group is only slightly more acidic than the carboxylic moiety, hence the concentrations of the microspecies AB and BA are at every pH fast equal (Figure 37).

REFERENCES

[1] Kukhar, V. P.; Hudson, H. R. (Eds.): Aminophosphonic and Aminophosphinic Acids; Wiley & Sons: New York, 2000.
[2] Meloun, M.; Havel, J.; Högfeldt, E. Computation of Solution Equilibria; Ellis Horwood: Chichester, 1988.
[3] Martell, A. E.; Motekaitis, R. J. The Determination and Use of Stability Constants; VCH: New York, 1988.
[4] Leggett, D. J. (Ed.): Computational Methods for the Determination of Formation Constants; Plenum Press: New York, 1986.
[5] Software development: (a) Hupperts, A. GENTIT; GENOPT, GENCOM, Diplomarbeit, Heinrich-Heine-Universität Düsseldorf, 1992; (b) Bier, A. ITERAX, Ph.D. Thesis, Heinrich-Heine-Universität Düsseldorf, Düsseldorf, Germany, 1993; (c) MINI_T: Bier, A. and Hägele, G. GIT Fachz Lab 1992, 6, 671; (d) NMR_T NMR_IT and AMPLSQ: Kropp, H. W.: Diplomarbeit, Heinrich-Heine-Universität Düsseldorf, Düsseldorf, Germany, 1994; (e) APBPLT, ASPPLT: Hägele, G. unpublished program.
[6] Preparative investigations: (a) Haas, A. Ph.D. Thesis, Heinrich-Heine-Universität Düsseldorf, Düsseldorf, Germany, 1996; (b) Becker, B. Ph.D. Thesis, Heinrich-Heine-Universität Düsseldorf, Düsseldorf, Germany, 1993; (c) Peters, J. Ph.D. Thesis, Heinrich-Heine-Universität Düsseldorf, Düsseldorf, Germany, 1992.
[7] NMR-controlled titrations: (a) Ollig, J. Ph.D. Thesis, Heinrich-Heine-Universität Düsseldorf, Düsseldorf, Germany, 1996; (b) Grzonka, M. Ph.D. Thesis, Heinrich-Heine-Universität Düsseldorf, Düsseldorf, Germany, 1989; (c) Hägele, G.; Grzonka, M.; Kropp, H.-W.; Ollig, J.; Spiegl, H. Phosphorus Sulfur Silicon 1993, 77, 85; (d) Hägele, G.; Varbanov, S.; Ollig, J.; Kropp, H.-W. Z Allg Anorg Chem 1994, 620, 914; (e) Hägele, G. NMR-Controlled Titrations of Phosphorus-Containing Acids and Bases in Protolysis and Complex Formation. In Phosphorus-^{31}P-NMR Spec-

tral Properties in Compound Characterization and Structural Analysis; Quin, L. D., Verkade, J. G., Eds.; VCH: New York, 1994; 395 pp. (f) Ollig, J.; Hägele, G. Comp Chem 1995, 19, 287; (g) Hägele, G.; Arendt, C.; Kropp, H. W.; Ollig, J. Phosphorus Sulfur Silicon 1996, 109, 205; (h) Papadopoulos, H. Ph.D. Thesis, Heinrich-Heine-Universität Düsseldorf, Düsseldorf, Germany, 1990.

[8] Hermens, S. unpublished results, 2000.

[9] Mohan, M. S.; Abbott, E. H. J Coord Chem 1978, 8, 175.

[10] Kiss, T.; Balla, J.; Nagy, G.; Kozlowski, H.; Kowalik, J. Inorg Chim Acta 1987, 138, 25.

[11] Schier, A.; Gamper, S.; Müller, G. Inorg Chim Acta 1990, 177, 179.

[12] Batchelor, J. G.; Feeney, J.; Roberts, G. C. J Magn Res 1975, 20, 19.

[13] Drenker, B. unpublished results, 2000.

[14] Szakács, Z. unpublished results, 2000.

[15] Pfaff, C. unpublished results, 2000.

[16] Topping, J.Errors of Observation and Their Treatment; Chapman and Hall: London, 1965, 38 pp.

[17] Sawada, K.; Araki, T.; Suzuki, T. Inorg Chem 1987, 26, 1199.

[18] Britt, H. I.; Luecke, R. H. Technometrics 1973, 15, 233.

[19] Fleisch, H. Drugs 1991, 42, 919.

[20] Lin, J. H.; Chen, I.; DeLuna, F. A. J Pharm Sci 1994, 83, 1741.

[21] Vega, D.; Baggio, R.; Garland, M. T. Acta Crystallographica (C) 1996, 52, 2198.

[22] Coiro, V. M.; Lamba, D. Acta Crystallographica (C) 1989, 45, 446.

[23] Leroux, Y.; El Manouni, D.; Safsaf, A.; Neuman, A.; Gillier, H. Phosphorus Sulfur Silicon 1991, 63, 181.

[24] Noszál, B. J Phys Chem 1986, 90, 4104.

[25] Szakács, Z.; Noszál, B. J Math Chem 1999, 26, 139.

[26] UV-vis controlled titrations: (a) Arendt, C.; Hägele, G. Comp Chem 1995, 19, 263; (b) Majer, H. J. Ph.D. Thesis, Heinrich-Heine-Universität Düsseldorf, Düsseldorf, Germany, 1993; (c) Hägele, G.; Majer, H. J.; Macco, F. GIT Fachz Lab 1992, 9, 922.

[27] Pillai, L.; Boss, R. D.; Greenberg, M. S. J Sol Chem 1979, 8, 635.

[28] Rabenstein, D. L. J Am Chem Soc 1973, 95, 2797.

[29] Mazák, K.; Nemes, A.; Noszál, B. Pharm Res 1999, 16, 1757.

[30] Noszál, B.; Visky, D.; Kraszni, M. J Med Chem 2000, 43, 2176.

[31] Noszál, B. Acid-Base Properties of Bioligands. In Biocoordination Chemistry, Burger, K., Ed.; Ellis Horwood: Chichester, New York, 1990; Chapter 11.

[32] Noszál, B.; Rabenstein, D. L. J Phys Chem 1991, 95, 4761.

[33] Rasche, E.; Cremer, J.; Donn, G.; Zink, J. The Development of Glufosinate Ammonium Tolerant Crops into the Market. In Brighton Crop Protection Conference; Weeds, Farnham, Surrey, U.K., 1995.